Wind-Tunnel Investigation
of the Flight Characteristics
# of a Canard General-Aviation
Airplane Configuration

Dale R. Satran

NASA

Wind-Tunnel Investigation of the Flight Characteristics of a Canard General-Aviation Airplane Configuration

Dale R. Satran

Langley Research Center
Hampton, Virginia

Summary

A 0.36-scale model of a canard general-aviation airplane with a single pusher propeller and winglets was tested in the Langley 30- by 60-Foot Wind Tunnel to determine the static and dynamic stability and control and free-flight behavior of the configuration. Model variables made testing of the model possible with the canard in high and low positions, with increased winglet area, with outboard wing leading-edge droop, with fuselage-mounted vertical fin and rudder, with enlarged rudders, with dual deflecting rudders, and with ailerons mounted closer to the wing tips.

The basic model exhibited generally good longitudinal and lateral stability and control characteristics. The removal of an outboard leading-edge droop degraded roll damping and produced lightly damped roll (wing rock) oscillations. In general, the model exhibited very stable dihedral effect but weak directional stability. Rudder and aileron control power were sufficiently adequate for control of most flight conditions, but appeared to be relatively weak for maneuvering compared with those of more conventionally configured models.

Introduction

As part of the NASA general-aviation stall/spin program, advanced aircraft configurations are being investigated that offer unique safety benefits. One such configuration, the Rutan VariEze, utilizes a high-aspect-ratio canard, a swept-back wing, winglets, and a pusher propeller. Full-scale flight tests of the homebuilt canard aircraft have demonstrated advantages for such a design from the standpoint of increased stall departure and spin resistance. (See ref. 1.) Several models of this configuration were tested in different facilities to document the flight characteristics of the VariEze. Reference 2 contains static wind-tunnel data for a full-scale model of the configuration tested in the Langley 30- by 60-Foot Wind Tunnel. Rotary-balance tests were conducted on a 0.22-scale model in the Langley Spin Tunnel, and the results showed the configuration to have inherently good stall departure and spin resistance. (See ref. 3.) In addition to improved safety features, the configuration has all-composite construction, which makes possible a smooth surface finish and, for this particular configuration, the realization of performance gains through large improvements in natural laminar flow. (See ref. 4.)

The purpose of this investigation was to use the free-flight test technique in the Langley 30- by 60-Foot Wind Tunnel to study the dynamic stability and control and general flight behavior of the configuration. A 0.36-scale model was used in the free-flight investigation and was also used to obtain static and dynamic force data to aid in the interpretation of the free-flight test results. The free-flight tests were conducted for angles of attack ranging from 7° to 14°. The investigation included tests of the model with high and low canard positions, three center-of-gravity locations, outboard wing leading-edge droop, winglets and a center vertical tail, and several roll- and yaw-control systems. Dynamic force tests were also conducted on the 0.36-scale model using the forced-oscillation test technique to study the effects of two canard vertical positions and using the installation of winglets and outboard leading-edge droop on the roll damping of the model. Wool tufts were installed to aid in flow visualization of the stall pattern of the wing and canard during the static force tests and free-flight tests.

Symbols

All longitudinal forces and moments are referenced to the stability-axis system, and all lateral-directional forces and moments are referenced to the body-axis system. The midpoint of the center-of-gravity range is $0.71\bar{c}$ ahead of the leading edge of the wing mean aerodynamic chord. (See fig. 1.) The wing reference area corresponds to that area obtained by extending the outboard leading and trailing edges of the wing without leading-edge droop to the fuselage centerline. All dimensional quantities are expressed in both the International System of Units (SI) and U.S. Customary Units. Measurements were made in U.S. Customary Units, and conversion factors from reference 5 were used to obtain equivalent SI dimensions.

b wing span, cm (in.)

C_D drag coefficient, $\frac{\text{Drag}}{qS}$

C_L lift coefficient, $\frac{\text{Lift}}{qS}$

C_l rolling-moment coefficient, $\frac{\text{Rolling moment}}{qSb}$

C_m pitching-moment coefficient, $\frac{\text{Pitching moment}}{qS\bar{c}}$

C_n yawing-moment coefficient, $\frac{\text{Yawing moment}}{qSb}$

C'_T effective thrust coefficient at zero angle of attack, $\frac{\text{Drag (power off)} - \text{Drag (power on)}}{qS}$

C_Y side-force coefficient, $\frac{\text{Side force}}{qS}$

$\bar{c}$ mean aerodynamic chord, cm (in.)

f frequency of oscillation, Hz

I_x	moment of inertia about X axis, kg-m^2 (slug-ft^2)
I_y	moment of inertia about Y axis, kg-m^2 (slug-ft^2)
I_z	moment of inertia about Z axis, kg-m^2 (slug-ft^2)
i_c	incidence angle of canard, positive trailing edge down, deg
k	reduced frequency parameter, $\omega b/2V$
p	roll rate, rad/sec
q	free-stream dynamic pressure, Pa (psf)
S	wing reference area, m^2 (ft^2)
V	free-stream velocity, m/sec (ft/sec)
y	spanwise coordinate, m (ft)
α	angle of attack, deg
β	angle of sideslip, deg
$\dot{\beta}$	rate of change of sideslip, rad/sec
ΔC_l	incremental rolling-moment coefficient (control deflected − control neutral)
ΔC_n	incremental yawing-moment coefficient (control deflected − control neutral)
ΔC_Y	incremental side-force coefficient (control deflected − control neutral)
δ_a	aileron deflection, positive for left roll, deg
δ_e	elevator deflection, positive for trailing edge down, deg
δ_f	flap deflection, positive for trailing edge down, deg
δ_r	rudder deflection, positive for left rudder trailing edge left, deg
ω	angular frequency, $2\pi f$, rad/sec

Stability derivatives:

$$C_{l_\beta} = \frac{\partial C_l}{\partial \beta} \qquad C_{n_\beta} = \frac{\partial C_n}{\partial \beta} \qquad C_{Y_\beta} = \frac{\partial C_Y}{\partial \beta}$$

$$C_{l_p} = \frac{\partial C_l}{\partial \frac{pb}{2V}} \qquad C_{n_p} = \frac{\partial C_n}{\partial \frac{pb}{2V}} \qquad C_{Y_p} = \frac{\partial C_Y}{\partial \frac{pb}{2V}}$$

$$C_{l_{\dot\beta}} = \frac{\partial C_l}{\partial \frac{\dot\beta b}{2V}} \qquad C_{n_{\dot\beta}} = \frac{\partial C_n}{\partial \frac{\dot\beta b}{2V}} \qquad C_{Y_{\dot\beta}} = \frac{\partial C_Y}{\partial \frac{\dot\beta b}{2V}}$$

Abbreviations:

BL	butt line
c.g.	center of gravity
FS	fuselage station
L.E.	leading edge
max	maximum
WL	waterline

Model and Apparatus

The basic configuration is depicted in a three-view diagram in figure 1, and photographs of the model are shown in figure 2. The mass and dimensional characteristics are included in table I. The 0.36-scale model is representative of the Rutan VariEze, a two-place, advanced general-aviation airplane. For all tests, the nose gear was retracted. The mass and inertial characteristics were scaled to correspond to operation at 1524 m (5000 ft) altitude (standard atmosphere). The wing, winglet, and canard of the model were constructed of balsa wood and fiberglass. The fuselage was made of fiberglass and foam sandwich construction with an internal aluminum structure.

The control surfaces were actuated for free-flight tests by electropneumatic servos. The controls consisted of a slotted canard flap used as an elevator, ailerons located inboard on the main wing, and rudders mounted on the winglets. The basic rudders deflected independently and outward only; that is, for a left turn, the trailing edge of the left rudder only would move to the left. The control deflections were limited during free-flight tests to ±20° for the ailerons, ±30° for the rudders, and ±5° for the elevator. Thrust to fly the model was supplied by a propeller driven by a turbine-air motor using compressed air.

Static force tests were made with several rudder modifications using sheet-metal tabs to simulate dual, split, and enlarged winglet rudders. These rudder modifications are shown in figure 3. The dual and split rudders had an area equivalent to that of the basic rudders. For dual-rudder control, both rudders deflected simultaneously and in the same direction; that is, for a left turn, the trailing edges of both rudders moved to the left. For split-rudder control, the inboard and outboard surfaces of one rudder split and deflected outward from the neutral position, and the rudder on the opposite winglet remained undeflected. The enlarged rudders operated in the same manner as the basic rudders, but had twice the chord, and extended in height to the tip of the winglets. The hinge line of the rudder was unchanged for all rudder modifications. A center vertical fin and conventional

rudder mounted on the fuselage directly ahead of the propeller were also tested.

Force tests were also conducted with outboard-mounted ailerons and with differential elevator deflection for roll control. The outboard ailerons were simulated using sheet-metal tabs mounted on the trailing edge of the wing on the outer 25 percent of the span. (See fig. 4.) Landing flaps were simulated in exploratory force tests by deflecting the ailerons symmetrically.

Tests were conducted with the canard mounted on the top of the fuselage, as the basic location, and with the canard mounted on the bottom of the fuselage, as an alternative location. Canard incidence was set at 0° and ±5° in both positions.

As a result of preliminary wind-tunnel testing and guidelines presented in reference 6, no. 60 grit was applied along the midchord of the upper surface of the canard to avoid laminar flow separation at the low test Reynolds numbers. Also incorporated into the basic configuration were wing leading-edge droop modifications on the outer 25 percent of the span. These droop modifications resulted in a wing chord extension of about 6 percent and a camber increase of 3 percent. The leading-edge droop modifications were similar to those in reference 7. A diagram of the airfoil-section modification and placement of the leading-edge droop is included in figure 4. Several tests were conducted with vortex generators located at the wing midchord, between the outboard end of the ailerons and the inboard end of the leading-edge droop, to investigate their effect on the stall characteristics of the wing. The vortex generators were sheet-metal tabs (1.27 cm (0.5 in.) square) angled ±45° to the free stream. (See fig. 4.)

During the investigation, the model produced an asymmetric stall with the right wing stalling at a lower angle of attack. Templates of the wing airfoil were made at several stations, and these templates showed that a discrepancy in the leading-edge radius had been built into the right wing panel. The contours are shown in figure 5. The effect of this model construction error is discussed in the section "Static Lateral-Directional Stability."

Testing Techniques

Static Force Tests

Static force tests were conducted in the Langley 30- by 60-Foot Wind Tunnel using a six-component strain-gauge balance mounted internally at the midpoint of the center-of-gravity range. Also, the canard was isolated from the aircraft by a second internal balance, so that simultaneous canard loads could be measured independently.

The static force data were measured at a nominal dynamic pressure of 464 Pa (9.7 psf), corresponding to a Reynolds number of 0.535×10^6 based on wing mean aerodynamic chord or 0.218×10^6 based on canard mean aerodynamic chord. The static force tests were conducted over an angle-of-attack range from $-10°$ to $90°$ and an angle-of-sideslip range of ±15°, although some of the tests were made over reduced angle-of-attack ranges. Static sideslip derivatives were determined from ±5° sideslip angles. Wind-tunnel flow-angularity corrections were applied to all data based on wind-tunnel flow surveys. Because the size of the model was small relative to that of the test section, no jet boundary corrections were included.

Forced-Oscillation Tests

Dynamic force tests were conducted using the forced-oscillation test equipment diagramed in figure 6. The model was mounted on a strut that forced the model to oscillate sinusoidally about the roll axis while an internal strain-gauge balance measured the forces and moments on the model. Reduction of the data provided measurements of the oscillatory stability derivatives that contain both damping and linear acceleration components. It has not been possible to accurately separate the two contributions, but experience has shown that reasonably good accuracy in dynamic stability calculations can be obtained using the combined form. The dynamic force test technique is discussed more fully in reference 8. The data reduction scheme is presented in the appendix of reference 9.

The model was tested in roll on the forced-oscillation apparatus at a dynamic pressure of 440 Pa (9.2 psf). A value of $k = 0.12$ was selected as representative of full-scale flight, which corresponds to a model oscillation frequency of 0.40 Hz at this dynamic pressure. The amplitude of the roll oscillations was ±5°; however, an amplitude of ±10° was also tested with no significant differences in the results. The model was tested with the canard in the high position with 0° incidence and in the low position with 5° incidence to correspond to the free-flight test configurations. Data were also taken with the canard off. With the canard in the high position, tests were made with the winglets installed and removed and with the leading-edge droop installed and removed.

Free-Flight Tests

In the free-flight test technique, two pilots fly the model within the open-throat test section of the Langley 30- by 60-Foot Wind Tunnel. Figure 7 is a diagram of the setup. A flexible flight cable supplies compressed air for power, transmits control signals,

and acts as a safety cable for the model. The flight cable is kept slack by a safety-cable operator using a high-speed, pneumatic winch. The roll and yaw pilot is located behind and below the test section; the pitch pilot and the throttle and safety-cable operators are located beside the test section. Rate gyros, accelerometers, and control-position potentiometers are mounted in the model, and the output of this instrumentation is sent to a flight-control computer. The flight-control computer receives the control inputs from the pilots and the information from the model instrumentation and combines them according to preprogrammed control laws that allow incorporation of automatic control mixing and artificial stabilization. A more complete discussion of this technique is contained in reference 8. For the present general-aviation study, rate gyros were installed in the model to provide a stable platform for convenience in exploratory studies, but all flights were repeated with gyros turned off.

The free-flight test results are in the form of pilot observations and motion-picture records of the handling qualities of the model. In addition to the qualitative observation of model motions, strip charts are used to record control input and model rates and accelerations.

The free-flight tests were conducted over a range of dynamic pressures from 402 to 263 Pa (8.4 to 5.5 psf) to investigate the dynamic response and flight characteristics for nominal angles of attack from 7° to 14°. These dynamic pressures correspond to a Reynolds number range from 0.498×10^6 to 0.403×10^6, based on wing mean aerodynamic chord. The model was tested with the canard in the high position at 0° incidence and with the wing leading-edge droop installed and removed. Also, tests were conducted with the canard in the low position at 0° and 5° incidence, but only with the wing leading-edge droop installed. Ballast was adjusted so that three center-of-gravity locations were tested: the basic location of $0.71\bar{c}$ ahead of the leading edge of the mean aerodynamic chord of the wing, and locations $0.10\bar{c}$ ahead of and behind the basic location.

Presentation of Results

The test results are presented in figures 8 to 35, which are grouped in order of discussion as follows:

Results of Static Force Tests

The static force data were measured to aid in the analysis and interpretation of the free-flight test results and are therefore discussed prior to the free-flight test results. The basic configuration was considered to have the canard in the high position and outboard leading-edge droop on the wing. The canard incidence was set at $0°$, and the data were presented for the mid c.g. location of $0.71\bar{c}$ ahead of the leading edge of the mean aerodynamic chord unless otherwise noted.

Static Longitudinal Stability and Control

The results of fluorescent oil-flow visualization tests indicated that substantial laminar boundary-layer separation occurred on the canard. This separation resulted in the highly nonlinear lift curve and high drag characteristics shown by the canard balance data in figure 8. Grit was applied to the mid-chord of the upper surface of the canard to minimize the flow separation, and all data presented herein were collected with grit applied to the canard. It should be noted that airfoils suffer performance degradation at low Reynolds numbers. Because of this degradation and the variance in Reynolds number between the full-scale airplane in flight and the 0.36-scale model in the wind tunnel, the results from the model do not reflect the performance of the full-scale airplane. However, results in the linear lift range should be representative of stability and control values. Results presented in reference 2 are for Reynolds numbers near flight conditions for the full-scale airplane and better predict the performance of the full-scale airplane.

Canard configurations require that the center of gravity be located between the canard center of lift and wing center of lift for positive stability and positive control. If the canard stalls before the wing stalls, longitudinal stability and airplane stall resistance are increased. The lift characteristics of the canard (fig. 9) indicate that the canard achieved maximum lift at an angle of attack slightly lower than that for model maximum lift. However, many factors must be considered in order to make a configuration stable and controllable as well as stall resistant.

The lift and pitching-moment data for the basic configuration (fig. 10) indicate that maximum elevator deflection for the mid c.g. position provided pitch trim for the model to $\alpha = 15°$, which is below wing stall. The canard is ineffective for trimming the model to an angle of attack beyond wing stall at the design mid c.g. location; therefore, the canard provides inherent angle-of-attack limiting at the mid c.g. position. For the forward c.g. position, the maximum elevator deflection provided pitch trim to $\alpha = 11°$, which still provides a C_L value of 1.2. The maximum elevator deflection for the aft c.g. position provided pitch trim to $\alpha = 30°$ with a potential deep-stall pitch-trim condition at $\alpha = 53°$. Figure 10(c) shows

5

that the model has sufficient elevator effectiveness at $\alpha = 53°$ to pitch the model out of the deep-stall trim point. As pointed out previously, the Reynolds number for this investigation was significantly lower than the Reynolds number for full-scale flight conditions. The data presented in reference 2 showed no deep-stall point.

The aerodynamic data for the low canard position are compared with data for the high canard position in figure 11(a), and the results indicate generally similar lift and pitching-moment characteristics for the two canard positions. The low canard position resulted in a small negative shift in angle of attack for $C_m = 0.0$. The drag characteristics presented in figure 11(b) do not change significantly with a change in the canard position, although drag measurements at this low Reynolds number are not directly applicable to full-scale flight.

The elevator effectiveness with the canard mounted in the low position is presented in figure 12 and indicates inherent angle-of-attack limiting, similar to that for the canard mounted in the high position. The low canard position resulted in some reduced static stability with the elevator deflected. This reduction was indicated by the reduced slope of the pitching-moment curve at approximately $\alpha = 8°$. This loss in stability with elevator deflection for the low canard position was not as apparent for the high canard position. (See fig. 9.) This loss in pitch stability may be associated with canard-wing interference, which occurred as a down load on the inboard wing and an upwash outboard on the wing. This adverse flow behavior of the canard on the wing was apparently more pronounced for the low canard configuration than for the high canard configuration.

The results of tests to show the effects of adjustment of canard incidence on the aerodynamic characteristics of the high and low canard configurations are presented in figure 13. The data show that increasing canard incidence to 5° increased the static stability of the configuration at higher angles of attack by causing the canard to stall in the region where partial wing stall would cause a reduction of static stability. The data of figure 13(b) show effects of incidence change for the low canard position similar to those for the high canard position. In choosing the proper canard incidence angle, consideration must be given to cruise drag penalties and stability characteristics. The low Reynolds numbers of the subject tests do not provide data suitable for such trade-off studies.

Results of tests to determine the effects of propeller thrust on the aerodynamic characteristics of the model are presented in figure 14. Figure 14 also shows that there were no significant thrust effects on the lift and pitching moment at low angles of attack,

apparently because the thrust line passed near the model center of gravity. At high angles of attack, the data show that thrust increased the lift and provided a stabilizing diving moment. This diving moment resulted partly from the induced slipstream effect over the wing, which increased the wing lift; however, the diving moment is probably caused mainly by the development of a propeller normal force by the rotating propeller disk, which on a pusher configuration produces a stabilizing moment.

Photographs showing the results of tuft studies on the model with and without the outboard wing leading-edge droop are presented in figure 15. These tuft photographs indicate that the installation of leading-edge droop significantly reduced the region of separated flow at the wing tips at high angles of attack. Data presented in figure 16(a) indicate unstable pitching-moment characteristics in the angle-of-attack range from about $\alpha = 5°$ to $\alpha = 15°$ for the model without the leading-edge droop. Installation of the leading-edge droop eliminated the unstable trends in the pitching-moment curve up to $\alpha = 30°$. The drag characteristics presented in figure 16(b) show no significant drag penalty for the installation of the leading-edge droop at positive lift coefficients at the test Reynolds number. The higher Reynolds number data of reference 2 indicated a cruise drag penalty of 0.0040 for the leading-edge droop.

Landing flaps were simulated by deflecting both ailerons symmetrically. Figure 17 indicates that flap deflections of 22° increased $C_{L,max}$ by 0.1 and decreased the angle at zero lift by 2°. However, flap deflection increased the nose-down pitching moment such that 20° elevator deflection trimmed to only $C_L = 1.0$, which is lower than the maximum trimmable C_L without flaps.

Static Lateral-Directional Stability

The static lateral-directional characteristics are presented as a function of sideslip angle in figure 18 and are generally linear with sideslip angle up to $\alpha = 18°$. The slopes of the data indicate a trend toward decreasing directional stability C_{n_β} and increasing the dihedral effect C_{l_β} with increasing angle of attack up to $\alpha = 14°$. The static lateral-directional coefficients at $\beta = 0°$ are presented in figure 19 and indicate that an asymmetry in roll and yaw to the right occurred through an angle-of-attack range from 15° to 25° that was not affected by the canard or leading-edge droop. Tuft studies indicated that the right wing stalled more abruptly than the left, and further investigation determined that a discrepancy in the leading-edge radius of the right wing of the model caused the asymmetric stall to occur.

The asymmetric stall was not a characteristic of the configuration, but was a result of inaccurate model construction on the right wing panel. As shown in figure 20, the asymmetric stall could be nearly eliminated by placing vortex generators at the midchord of the wing or by extending the leading-edge droop inboard to the region of the discrepancy.

The effects of the winglets on the static lateral-directional stability derivatives are presented in figure 21. The basic configuration exhibited stable dihedral effect, due to wing sweep, that increased linearly with angle of attack up to $\alpha = 14°$. The winglets provided a constant increment to C_{l_β}. Above $\alpha = 14°$, C_{l_β} was reduced sharply due to the asymmetric stall noted previously. Normally, C_{l_β} would be expected to increase linearly with angle of attack in the region where lift is a linear function of angle of attack ($\alpha < 16°$). The directional stability of the basic configuration decreased linearly from moderate stability at $\alpha = 0°$ to neutral stability at $\alpha = 14°$. Above $\alpha = 14°$, C_{n_β} increased sharply to $\alpha = 20°$ and then decreased and became unstable at high angles of attack. The increment to C_{n_β} from the winglets decreased with increasing angle of attack.

The effects of wing leading-edge droop on the lateral-directional characteristics of the model are shown in figure 22. The leading-edge droop made no significant contribution to the static lateral-directional stability at low-to-moderate angles of attack. In the post-stall region, the droop provided flow attachment at the wing tips which improved C_{l_β}, although C_{n_β} was generally degraded.

The effect of the canard on lateral-directional stability is presented in figure 23(a), and the data indicate that the canard had no significant effect on C_{l_β} but degraded C_{n_β} below stall in either the high or low position. In the post-stall angle-of-attack region, the high canard was very destabilizing directionally but provided a stabilizing increment to lateral stability. The data of figure 23(b) show that deflecting the canard elevator produced little effect on the lateral-directional stability characteristics. The increase in C_{l_β} produced by the canard is probably due to the canard downwash being asymmetric on the wing when the configuration is sideslipped.

Increased winglet area and a center vertical tail were tested to provide increased directional stability; the results are presented in figure 24. The data of figure 24 show that the center tail provided a constant increment of C_{n_β} of about 0.005 that was not affected by thrust changes, despite the close proximity of the propeller to the tail. The enlarged winglets provided a substantial increase in C_{n_β} and increased

the angle of attack at which C_{n_β} became unstable. Neither the center tail nor enlarged winglets affected C_{l_β} significantly up to the stall angle of attack.

Static Lateral-Directional Control

The results of tests to determine the lateral control power are presented in terms of ΔC_Y, ΔC_n, and ΔC_l produced by a right-roll or right-yaw control input. Data showing aileron effectiveness are presented in figure 25 and indicate that the available roll control decreased with increasing angle of attack, probably because of the progression of separated flow into the region of the ailerons. Aileron deflection exhibited favorable yawing moments from $\alpha = 0°$ to $\alpha = 14°$, above which the yawing moment became adverse. The canard vertical position produced only minor effects on the aileron control data.

The roll-control characteristics of simulated ailerons mounted outboard, behind the leading-edge droop, are compared with data for the basic ailerons in figure 26. As expected from the increased lateral-moment arm, the outboard ailerons greatly increased the available roll control up to $\alpha = 25°$. However, the outboard ailerons caused moderate values of adverse yaw below $\alpha = 8°$ but eliminated the adverse yaw characteristics of the basic ailerons in the stall region.

Differential elevator deflection to provide roll control is compared with the basic aileron effectiveness in figure 27(a); canard balance data are included for comparison with model balance data. Figure 27(a) shows that differential elevator control was less effective than the basic ailerons. Below $\alpha = 16°$, the canard downwash altered the local angle of attack of the wing such that the wing produced an opposing rolling moment. Above $\alpha = 16°$, the wing was stalled, and the rolling moment measured by the canard balance was equal to that of the model balance. Differential elevator deflection for the low canard (fig. 27(b)) indicates similar results to those of the high canard. The yawing moments produced by differential elevator deflection were more adverse for the low canard position than for the high canard position.

Data showing rudder effectiveness are presented in figure 28 and indicate that the yawing moment produced by rudder deflection was approximately linear with rudder deflection. The rudder effectiveness remained almost constant with angle of attack up to $\alpha = 10°$ and then decreased linearly through the stall. Comparison of the data of figures 18 and 28 indicates sufficient rudder control up to fairly large sideslip angles. Comparison of the winglet rudder data to data measured for a rudder mounted on a center vertical tail (fig. 29) indicates that the

center rudder produced approximately half as much yaw control as the winglet rudders. There were slight power effects on the center rudder for climb power conditions ($C'_T = 0.39$).

Three modifications to the winglet rudders were tested (as noted in the section "Model and Apparatus"), and the results are presented in figure 30. The enlarged rudders and the dual-rudder deflections increased the available yaw control. The split rudders, however, provided a reduction in yaw control. Further testing indicated that the reason for the adverse control effect from the split rudder was that the drag from the split rudder, which was the mechanism expected to yaw the model in the direction of the split rudder, was offset by the reduction in inward side force normally produced by that winglet. The inward side force from the opposite winglet was greater than that produced from the split-rudder winglet. The net effect was that the yaw control was opposite to that desired.

Results of Forced-Oscillation Tests

The roll forced-oscillation tests were conducted to measure the oscillatory stability derivatives $C_{Y_p} + C_{Y_{\dot\beta}} \sin \alpha$, $C_{n_p} + C_{n_{\dot\beta}} \sin \alpha$, and $C_{l_p} + C_{l_{\dot\beta}} \sin \alpha$, and the results of the tests are presented in figures 31 to 33. Roll damping $C_{l_p} + C_{l_{\dot\beta}} \sin \alpha$ was of primary interest because of wing rock oscillations encountered in the free-flight testing.

The leading-edge droop was installed to prevent premature wing-tip stall that was found in static tuft studies. The data of figure 31 show a loss of roll damping without the leading-edge droop and unstable roll damping at $\alpha = 16°$. The addition of the leading-edge droop helped to maintain attached flow at the wing tips and provided stable roll damping throughout the angle-of-attack range.

The data of figure 32 show that the canard position had little effect on roll stability. The roll damping was progressively reduced as angle of attack increased, and the canard position did not affect this trend. The roll damping remained stable throughout the angle-of-attack range with the canard in either position, although the damping decreased in the angle-of-attack range from 15° to 20°.

The effect of winglets on the roll oscillation data is shown in figure 33. The data show that the winglets had little effect on roll damping at the lower angles of attack. The main effect of the winglets was to provide a negative increment to $C_{n_p} + C_{n_{\dot\beta}} \sin \alpha$ over the test angle-of-attack range. For the low-angle-of-attack range, this negative increment to $C_{n_p} + C_{n_{\dot\beta}} \sin \alpha$ results in an adverse yawing moment due to rolling.

Results of Free-Flight Tests

The majority of the free-flight tests were conducted with augmented roll-, yaw-, and pitch-rate damping to provide a stable platform for ease of flying while conducting exploratory studies. However, flights performed without stability augmentation indicated that there were no significant changes in the trends or overall flight characteristics other than a reduction in the workload of the pilot that was required to control the model. Where applicable, the results of the free-flight tests are compared with those of the static and dynamic force tests previously discussed. Since the free-flight tests were conducted at lower Reynolds numbers than the static force tests, some characteristics, such as local flow separation, may occur at slightly different angles of attack.

Late in the flight-test program, when high-angle-of-attack stall flight tests were attempted, an asymmetry between the left and right wing panels was detected. The asymmetry caused the model to depart in yaw to the right at an angle of attack of 14° for all test conditions. No free-flight tests were conducted after fixes for the asymmetry were found.

Longitudinal Flight Characteristics

The basic configuration with the high canard was stable and well damped in pitch but was sensitive to elevator control inputs, particularly for nose-down control. The model dropped and pitched rapidly from trimmed flight with slight nose-down elevator deflection. Elevator deflection required for trimmed flight varied linearly from $\delta_e = 6°$ at $\alpha = 9°$ to $\delta_e = 14°$ at $\alpha = 14°$ for the mid c.g. position. The model had good pitch stability at the aft center-of-gravity location, but the workload of the pilot increased significantly because of increased elevator sensitivity. Any attempt to fly at higher angles of attack, particularly at the aft c.g. position, was expected to give less desirable pitch stability characteristics. The model was not flown above $\alpha = 14°$ because of an asymmetry between the left and right wing panels (fig. 5), which caused the model to depart in yaw to the right at $\alpha = 14°$. This departure was not characteristic of the airplane and was strictly a characteristic of the model.

The removal of the leading-edge droop did not significantly affect the longitudinal flight characteristics for the limited angle of attack investigated. The static force data presented in figure 16 indicate that, with the droop removed, a destabilizing break occurred in the pitching-moment curve at angles of attack near stall. However, the model exhibited no pitch instability with the leading-edge droop removed at the lower angles of attack. Longitudinal power ef-

8

fects were not significant. As demonstrated by the static data presented in figure 14, the pitching moment was not affected by thrust changes in the free-flight test angle-of-attack range.

Flights made with the low canard position indicated that the longitudinal flight characteristics were similar to those with the high canard. The model displayed similar pitch stability and elevator sensitivity. The static data presented in figure 11 indicate a slight nose-down shift in the pitching moment because of the low canard. This shift was demonstrated by a $2°$ to $3°$ increase in the elevator deflection required to trim the model with the low canard throughout the angle-of-attack range tested. To reduce the trim elevator deflection with the low canard, flight tests were also conducted with $5°$ canard incidence. The trim elevator deflection was reduced by $3°$ to $4°$ with the increased canard incidence. Static data presented in figure 13 indicate an increase in static stability and a slight reduction in elevator sensitivity with $5°$ incidence. These results were verified in the flight tests. The flights with $5°$ canard incidence were much steadier, and the model did not display the elevator sensitivity found with the high canard or the low canard with $0°$ incidence.

Lateral-Directional Flight Characteristics

The basic configuration with the high canard and leading-edge droop installed exhibited adequate directional stability and stable dihedral effect, as shown in the static data of figure 21. The model motions were stable and well damped in roll and yaw under $\alpha = 14°$. At $\alpha = 14°$, the model departed in roll and yaw to the right as the result of an asymmetric stall brought on by an airfoil asymmetry between the right and left wing panels.

The basic lateral-directional control power was sufficient for adequate control of the model, although the pilot noted that the rudder effectiveness was relatively weak for maneuvering and recovering from disturbances. The flight tests showed that the basic ailerons produced noticeable adverse yaw, particularly above $\alpha = 9°$. The static force data in figure 25 indicate adverse yaw at angles of attack between $15°$ and $20°$. Adverse yaw is usually related to local flow separation on the wing panel with the aileron deflected down. Since the free-flight tests were conducted at lower Reynolds numbers than the static force tests, the adverse yaw was probably occurring at lower angles of attack. In all cases, the adverse yaw could be compensated for by rudder deflection. The rudder effectiveness was sufficient to control the model without aileron input at lower angles of attack because of the large bank angles that could be induced by the strong favorable dihedral effect. At

angles of attack greater than $11°$, the rudder effectiveness was not sufficient to recover the model from large disturbances without the addition of aileron deflection. Recovery from the departure at $\alpha = 14°$ due to wing asymmetric stall could not be made with the available aileron and rudder control. The aft center-of-gravity position resulted in reduced control effectiveness and more erratic flight behavior.

Removal of the leading-edge droop caused definite deterioration of flight characteristics in both roll and yaw. At $\alpha = 0°$, the model behaved much the same as with the droop installed, but with reduced damping in roll. At $\alpha = 11°$, wing rock could be easily induced by small aileron or rudder deflections. The oscillation was stable but only slightly damped, which correlates with the forced-oscillation results of figure 31 that indicate unstable roll damping with the droop removed.

The model flew steadier in pitch with the low canard at $5°$ incidence, which resulted in a reduced workload for the lateral-directional pilot. No significant difference was seen in the lateral-directional flight characteristics for the low or high canard configurations. This result was expected, since the static and dynamic force tests indicated that the low canard position did not alter the static or dynamic lateral-directional force characteristics.

The enlarged winglet rudders and center tail were tested to increase the directional stability and rudder effectiveness. The static data of figures 24, 29, and 30 show the improvements in directional stability and rudder control, and these improvements were supported by the free-flight tests. Although the model had improved flight characteristics below the stall, the increased directional stability and rudder effectiveness were not sufficient to prevent departure at $\alpha = 14°$ because of the wing contour asymmetry problem.

Interpretation of Results

The results of the free-flight tests for this configuration showed generally good agreement with the static force test data. The asymmetry in the model limited the angle-of-attack range in which testing could be performed but did not affect the results unless otherwise noted. Of course, the low Reynolds numbers associated with the present tests could cause some characteristics, such as local flow separation, to occur at slightly different angles of attack under different test conditions. Also, the confined space available within the wind tunnel, the rapidity of the motions of the model, and the lack of piloting cues cause the evaluation of the longitudinal and lateral-directional control techniques to be qualitative at best.

To better evaluate the free-flight test data, calculations were made using linear analysis techniques of three-degree-of-freedom lateral-directional equations of motion. Included in the computations are response estimates for a representative conventional low-wing configuration (ref. 10) for comparison with the response estimate of the advanced-canard configuration. The results of calculated response due to aileron and rudder inputs are presented in figures 34 and 35. The data of figure 34 show that the aileron roll response for the basic canard configuration was lower than that of the conventional configuration at low lift coefficients and about equal for the two configurations at high lift coefficients. Modifying the canard design with ailerons located outboard provided more aileron response for the canard design at low and high lift coefficients. The rudder response data of figure 35 show that the yaw response from rudder deflection was much lower for the canard design than for the representative conventional design. Enlarging the winglets provided some improvement in rudder response of the canard design, but the response was still much lower than that of the conventional design, particularly at high lift coefficient corresponding to climb condition. The greater response of the conventional design in this analysis was due to the fact that the conventional design had a much greater moment arm to the rudder and that the propeller slipstream effects were very favorable with the tractor arrangement in the conventional design at climb lift coefficients. Although the conventional design has larger directional control power, the canard configuration is also controllable. This is partly a result of the lower levels of lateral-directional stability of the canard configuration.

Conclusions

An investigation of the static and dynamic longitudinal and lateral-directional characteristics of a canard general-aviation aircraft configuration was conducted. The following conclusions were reached as a result of this investigation.

1. During free-flight tests, adequate pitch stability was demonstrated throughout the angle-of-attack range from 7° to 14° for the rearmost center-of-gravity position, but the model was more sensitive to elevator deflection at moderate angles of attack.

2. A low canard configuration offered flight characteristics similar to those of the high canard configuration but required an adjustment in canard incidence angle of 5° for improved flight behavior.

3. The model exhibited a strong favorable dihedral effect but low directional stability. The addition of a fuselage-mounted vertical fin increased the directional stability, as did enlarged winglets. The lateral-

directional characteristics were not significantly affected by canard vertical position.

4. The addition of an outboard wing leading-edge droop prevented premature wing-tip stall and, as a result, increased the roll damping and eliminated a wing rock tendency at high angles of attack.

5. Roll control from the basic inboard ailerons was sufficient to control the model in free-flight tests. Outboard-mounted ailerons improved aileron effectiveness but increased adverse yaw.

6. Sufficient rudder control was available for steady flight conditions. The rudder effectiveness was increased by dual deflection of the basic rudders or by increased rudder area.

7. A three-degree-of-freedom lateral-directional equations-of-motion study indicated weak lateral-directional control power, especially when the rudder effectiveness was compared with a conventional low-wing general-aviation configuration.

References

1. Rutan, Burt: VariViggen/VariEze Canard Designs for Flying Qualities and Performance. *Homebuilt Experimental Aircraft Theory and Practice*, First ed., William E. Vasen, ed., Western Periodicals Co., c.1975, pp. 119 126.

2. Yip, Long P.: *Wind-Tunnel Investigation of a Full-Scale Canard-Configured General Aviation Airplane*. NASA TP-2382, 1985.

3. Bihrle, William, Jr.; and Bowman, James S., Jr.: Influence of Wing, Fuselage, and Tail Design on Rotational Flow Aerodynamics Beyond Maximum Lift. *J. Aircr.*, vol. 18, no. 11, Nov. 1981, pp. 920 925.

4. Holmes, Bruce J.; Obara, Clifford J.; and Yip, Long P.: *Natural Laminar Flow Experiments on Modern Airplane Surfaces*. NASA TP-2256, 1984.

5. *Standard for Metric Practice*. E 380-79, American Soc. Testing & Mater., c.1980.

6. Braslow, Albert L.; and Knox, Eugene C.: *Simplified Method for Determination of Critical Height of Distributed Roughness Particles for Boundary-Layer Transition at Mach Numbers From 0 to 5*. NACA TN 4363, 1958.

7. Staff of the Langley Research Center: *Exploratory Study of the Effects of Wing-Leading-Edge Modifications on the Stall/Spin Behavior of a Light General Aviation Airplane*. NASA TP-1589, 1979.

8. Parlett, Lysle P.; and Kirby, Robert H.: Test Techniques Used by NASA for Investigating Dynamic Stability Characteristics of V/STOL Models. *J. Aircr.*, vol. 1, no. 5, Sept. Oct. 1964, pp. 260 266.
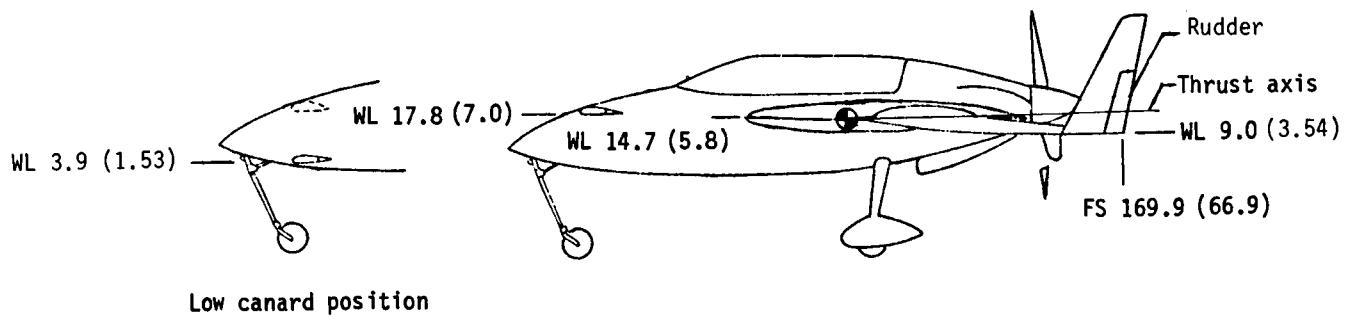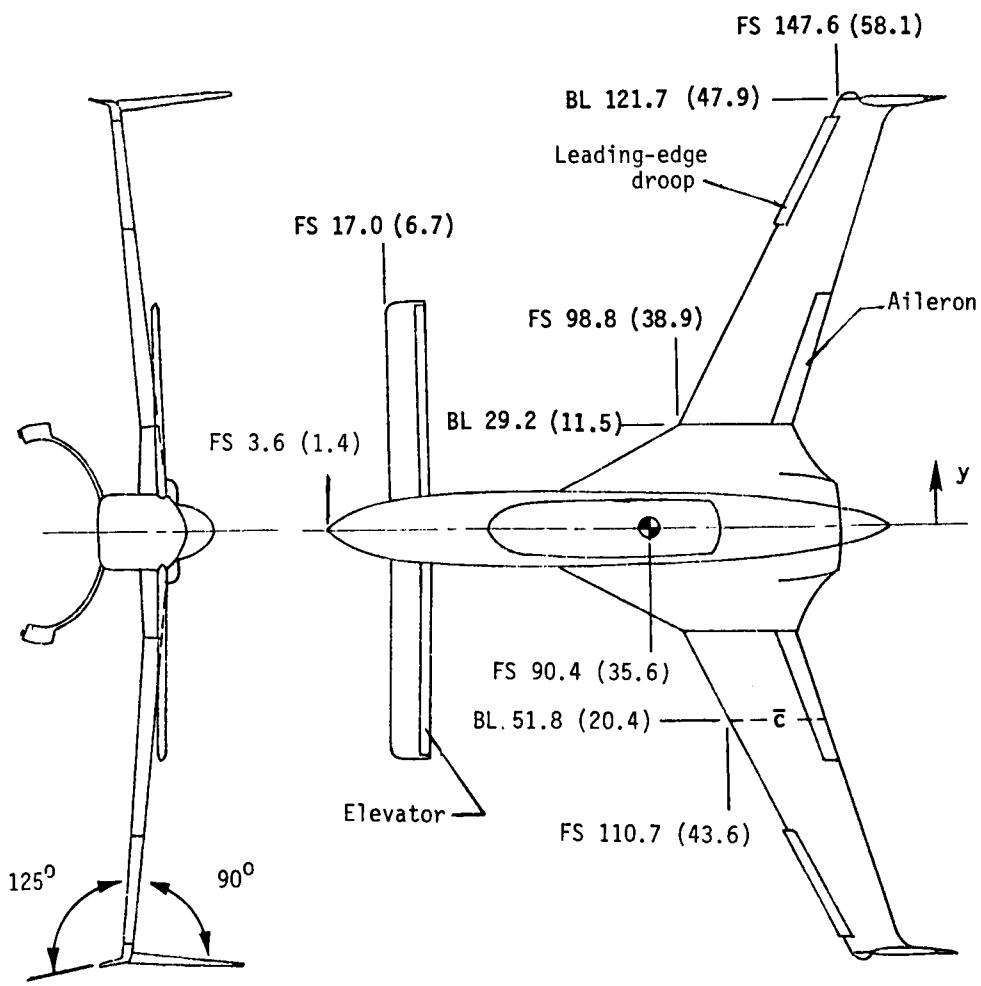
9. Chambers, Joseph R.; and Grafton, Sue B.: *Static and Dynamic Longitudinal Stability Derivatives of a Powered 1/9-Scale Model of a Tilt-Wing V/STOL Transport.* NASA TN D-3591, 1966.

10. Newsom, William A., Jr.; Satran, Dale R.; and Johnson, Joseph L., Jr.: *Effects of Wing-Leading-Edge Modifications on a Full-Scale, Low-Wing General Aviation Airplane—Wind-Tunnel Investigation of High-Angle-of-Attack Aerodynamic Characteristics.* NASA TP-2011, 1982.

11. Kelling, F. H.: *Experimental Investigation of a High-Lift Low-Drag Aerofoil.* C.P. No. 1187, British A.R.C., 1971.

TABLE I. MASS AND GEOMETRIC CHARACTERISTICS OF MODEL

Weight, N (lb) 230.2 (51.75)

Moments of inertia:

   I_x, kg-m^2 (slug-ft^2) 1.818 (1.341)

   I_y, kg-m^2 (slug-ft^2) 4.233 (3.122)

   I_z, kg-m^2 (slug-ft^2) 5.713 (4.214)

Fuselage:

   Overall length, cm (in.) 167.34 (65.88)

   Mid center-of-gravity location, nose to c.g., cm (in.) 87.10 (34.29)

Wing:

   Span, cm (in.) 243.84 (96.00)

   Area, cm^2 (in^2) 6449.7 (999.7)

   Centerline chord, cm (in.) 38.40 (15.12)

   Root chord, cm (in.) 32.92 (12.96)

   Tip chord, cm (in.) 14.63 (5.76)

   Mean aerodynamic chord, $\bar{c}$, cm (in.) 28.32 (11.15)

   Spanwise location of $\bar{c}$, cm (in.) 51.71 (20.36)

   Longitudinal location of $\bar{c}$, cm (in.) . . . . FS 110.7 (43.6)

   Aspect ratio 9.18

   Taper ratio 0.381

   Sweepback angle of quarter-chord, deg 25.7

   Dihedral angle, deg . . . . −4

   Incidence angle at root, deg 1.2

   Incidence angle at tip, deg . . . . −1.8

   Airfoil section . . . . GA(W)-1 (modified)

Aileron (per side):

   Area, cm^2 (in^2) 241.9 (37.49)

   Span, cm (in.) 36.63 (14.42)

   Inboard end chord, cm (in.) 6.50 (2.56)

   Outboard end chord, cm (in.) 5.54 (2.18)

Canard:

   Area, cm^2 (in^2) 1580.6 (245.0)

   Span, cm (in.) 137.16 (54.00)

   Chord (constant), cm (in.) 11.53 (4.54)

   Sweepback angle of quarter-chord, deg 0

   Aspect ratio 11.90

   Airfoil section (ref. 11) . . . . GU25-5(11)8

TABLE I. Concluded
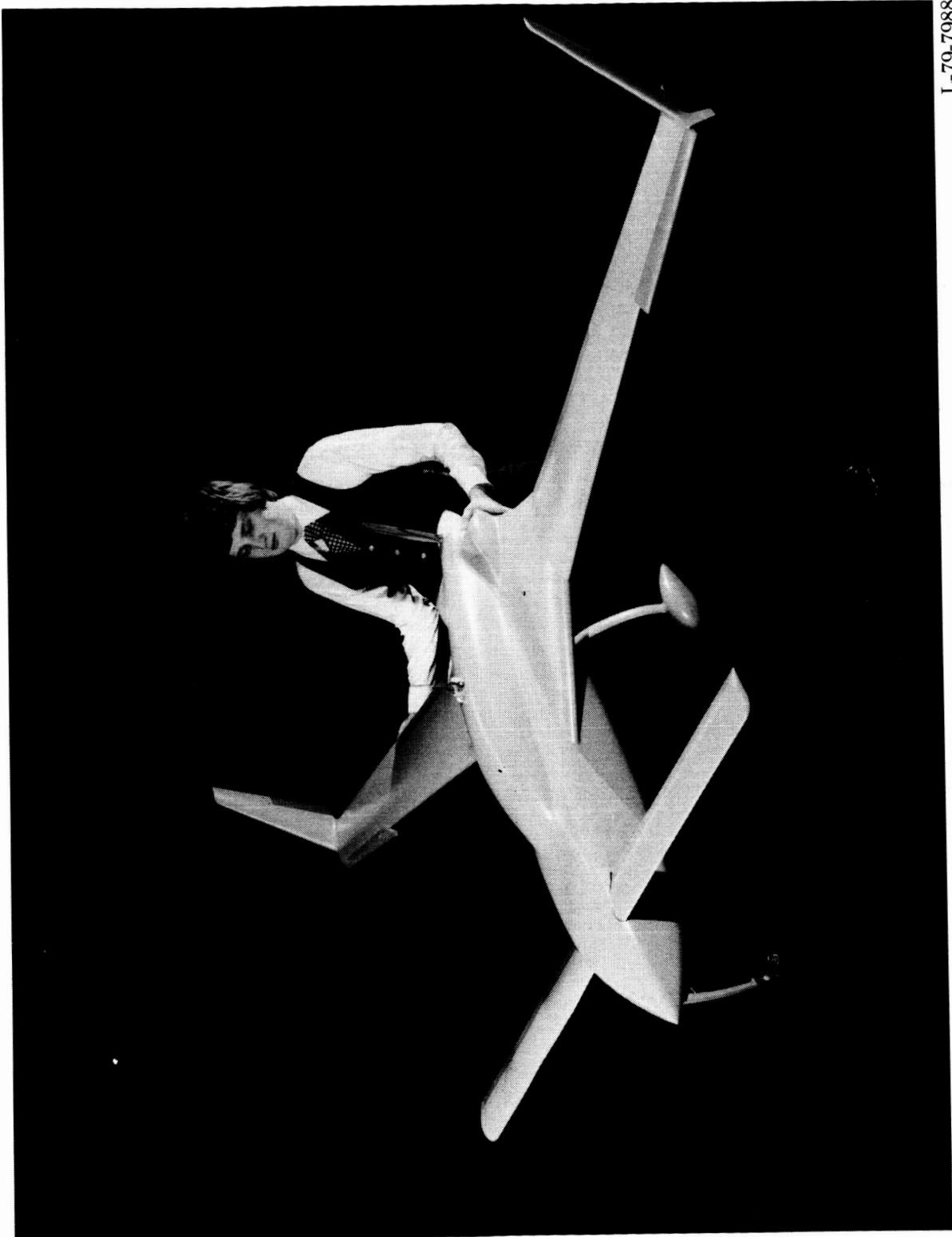
Elevator:

    Area, cm^2 (in^2) 453.1 (70.23)

    Span, cm (in.) 137.67 (54.20)

    Chord, cm (in.) 3.30 (1.30)

Upper winglet (per side):

    Area, cm^2 (in^2) 407.0 (63.08)

    Span, cm (in.) 32.92 (12.96)

    Root chord, cm (in.) 18.29 (7.20)

    Tip chord, cm (in.) 6.40 (2.52)

    Aspect ratio 2.66

    Sweepback angle of quarter-chord, deg 26.3

    Dihedral angle (from horizontal), deg 86.0

    Incidence angle at root, deg 0

    Incidence angle at tip, deg . . . . −1.0

Rudder:

    Area, cm^2 (in^2) 89.6 (13.89)

    Span, cm (in.) 17.88 (7.04)

    Lower-end chord, cm (in.) 5.49 (2.16)

    Upper-end chord, cm (in.) 4.52 (1.78)

Lower winglet (per side):

    Area, cm^2 (in^2) 47.2 (7.31)

    Span, cm (in.) 6.38 (2.51)

    Root chord, cm (in.) 4.62 (1.82)

    Tip chord, cm (in.) 2.74 (1.08)

    Sweepback angle of quarter-chord, deg 12

    Dihedral angle (from horizontal), deg . . . . −60

FS 147.6 (58.1)

BL 121.7 (47.9)

Leading-edge droop

FS 17.0 (6.7)

FS 98.8 (38.9)

Aileron

FS 3.6 (1.4)

BL 29.2 (11.5)

y

FS 90.4 (35.6)

BL.51.8 (20.4)

c̄

Elevator

FS 110.7 (43.6)

125°   90°

Rudder

WL 17.8 (7.0)

Thrust axis

WL 14.7 (5.8)

WL 9.0 (3.54)

WL 3.9 (1.53)

FS 169.9 (66.9)

Low canard position

Figure 1. Three-view diagram of model with mid c.g. position shown. Linear dimensions are in cm (in.).

L-79-7988

(a) High canard position with wing leading-edge droop installed.

Figure 2. Photographs of model.

15
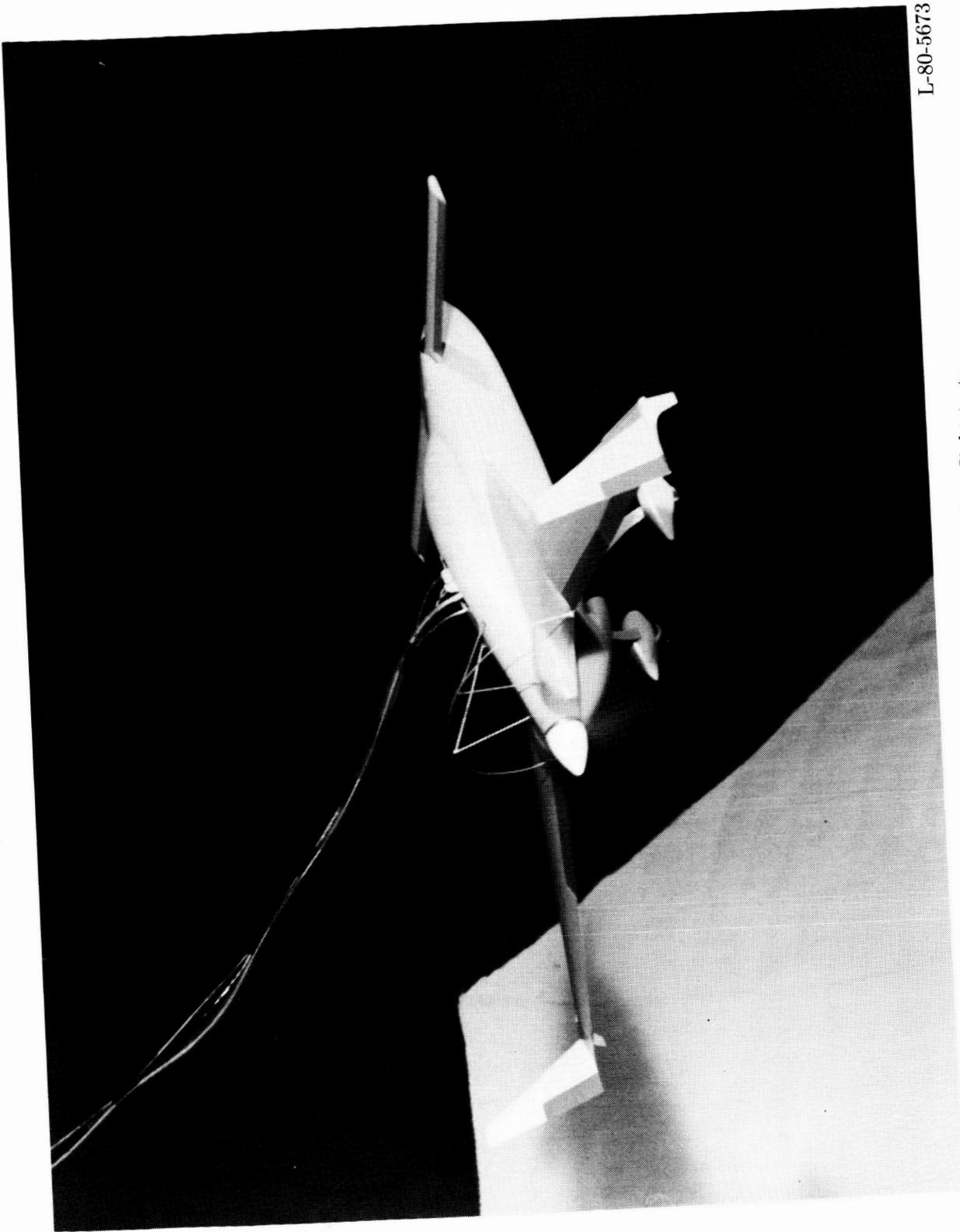
L-79-7989

(b) Low canard position with wing leading-edge droop removed.

Figure 2. Continued.

L-80-5673

(c) High canard configuration in free-flight tests.

Figure 2. Concluded.

17
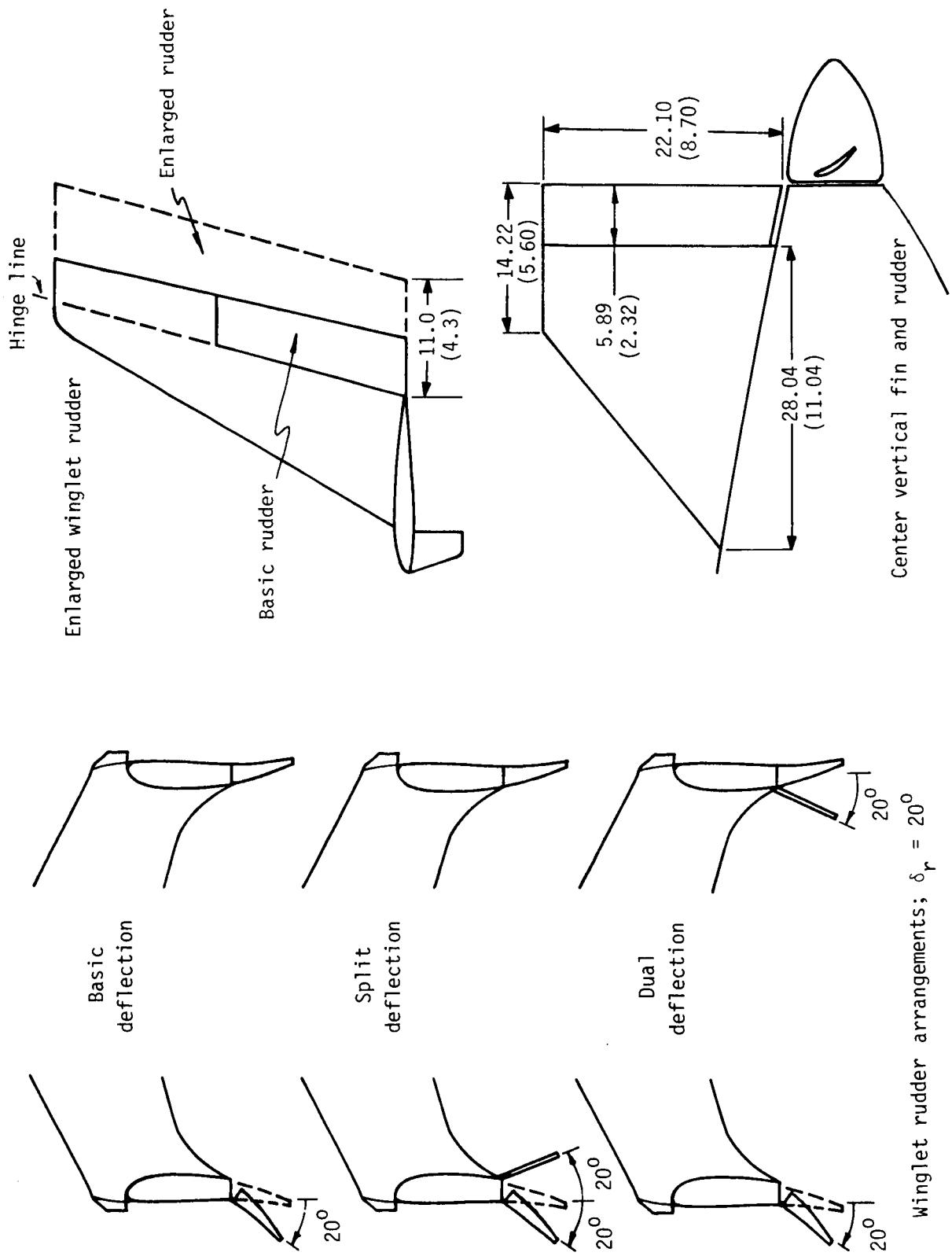
Figure 3. Rudder modifications. Linear dimensions in cm (in.).

18
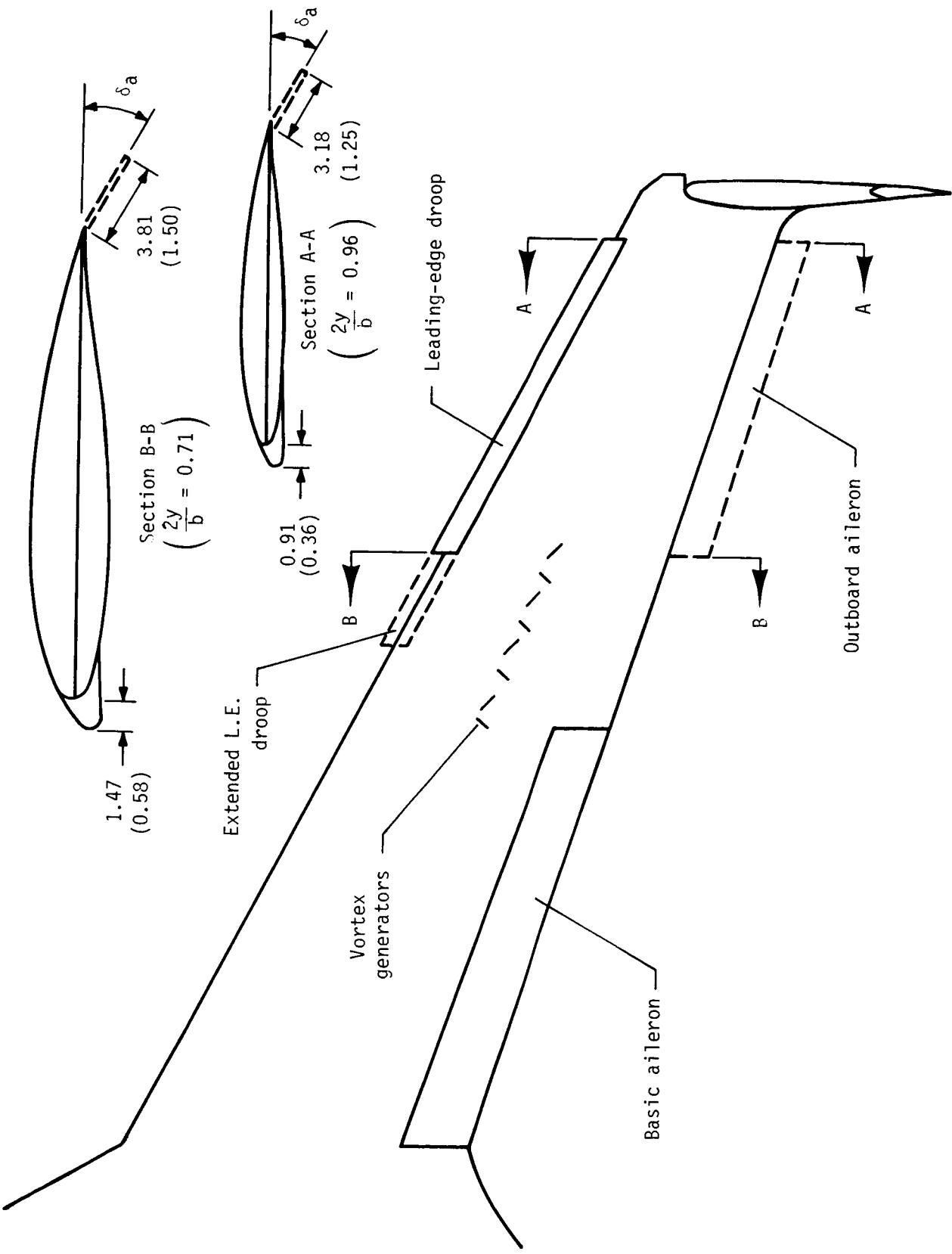
Figure 4. Wing modifications. Linear dimensions in cm (in.).

δ_a

3.81
(1.50)

Section B-B
$\left(\dfrac{2y}{b} = 0.71\right)$

δ_a

3.18
(1.25)

Section A-A
$\left(\dfrac{2y}{b} = 0.96\right)$

0.91
(0.36)

1.47
(0.58)

Extended L.E.
droop

Leading-edge droop

A

A

B

B

Vortex
generators

Outboard aileron

Basic aileron
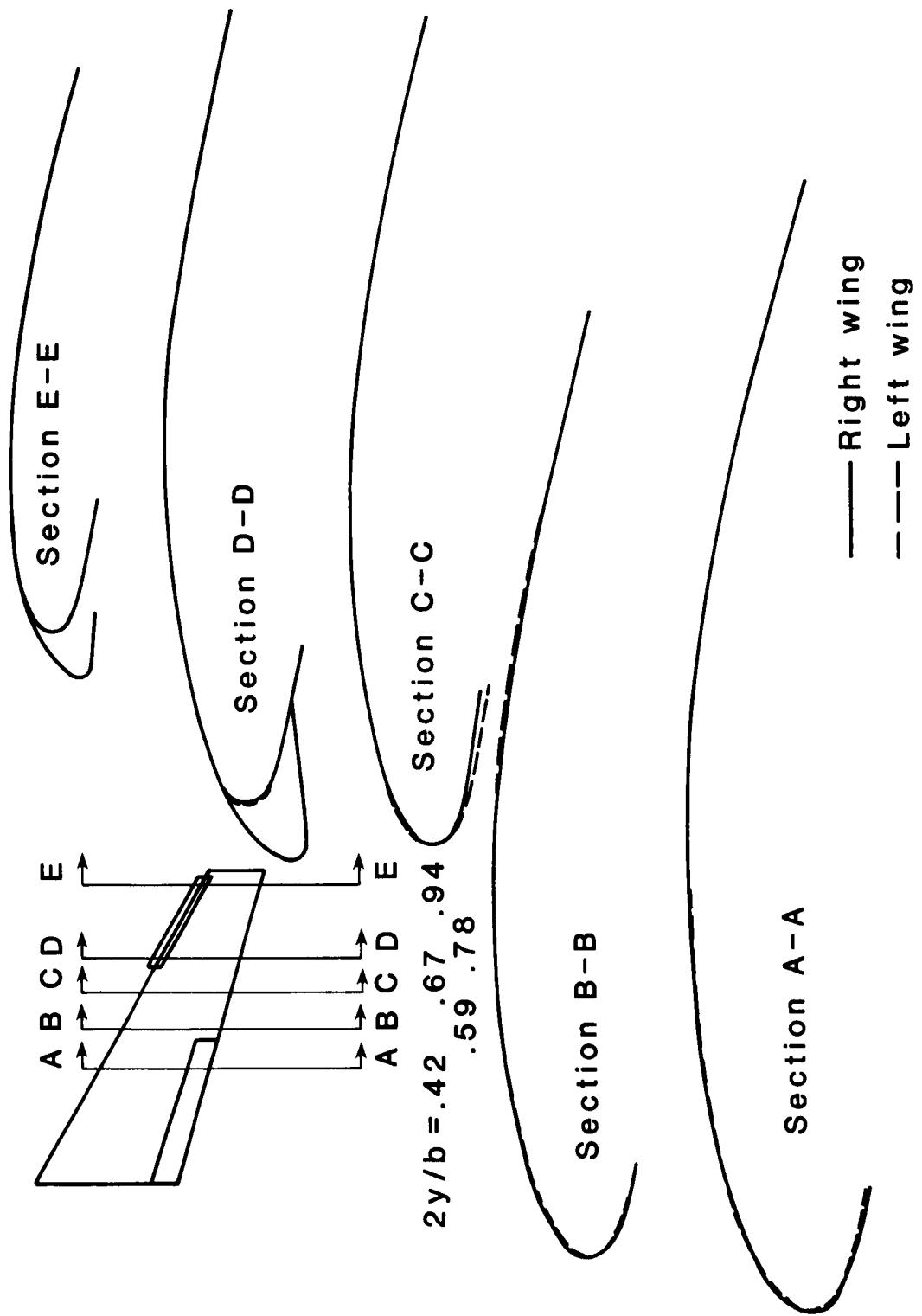
Figure 5. Wing leading-edge contours.
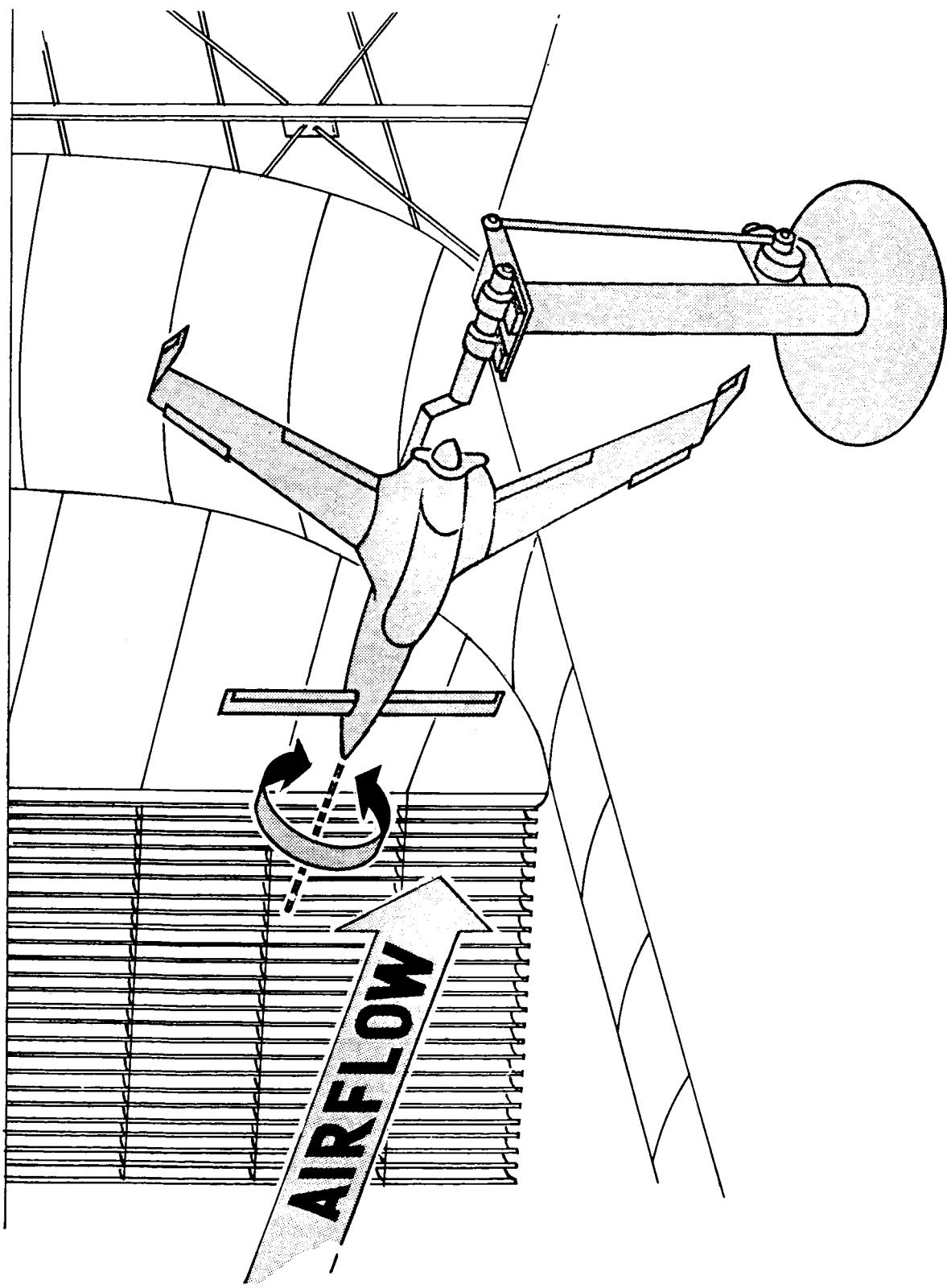
Figure 6. Forced-oscillation test apparatus.
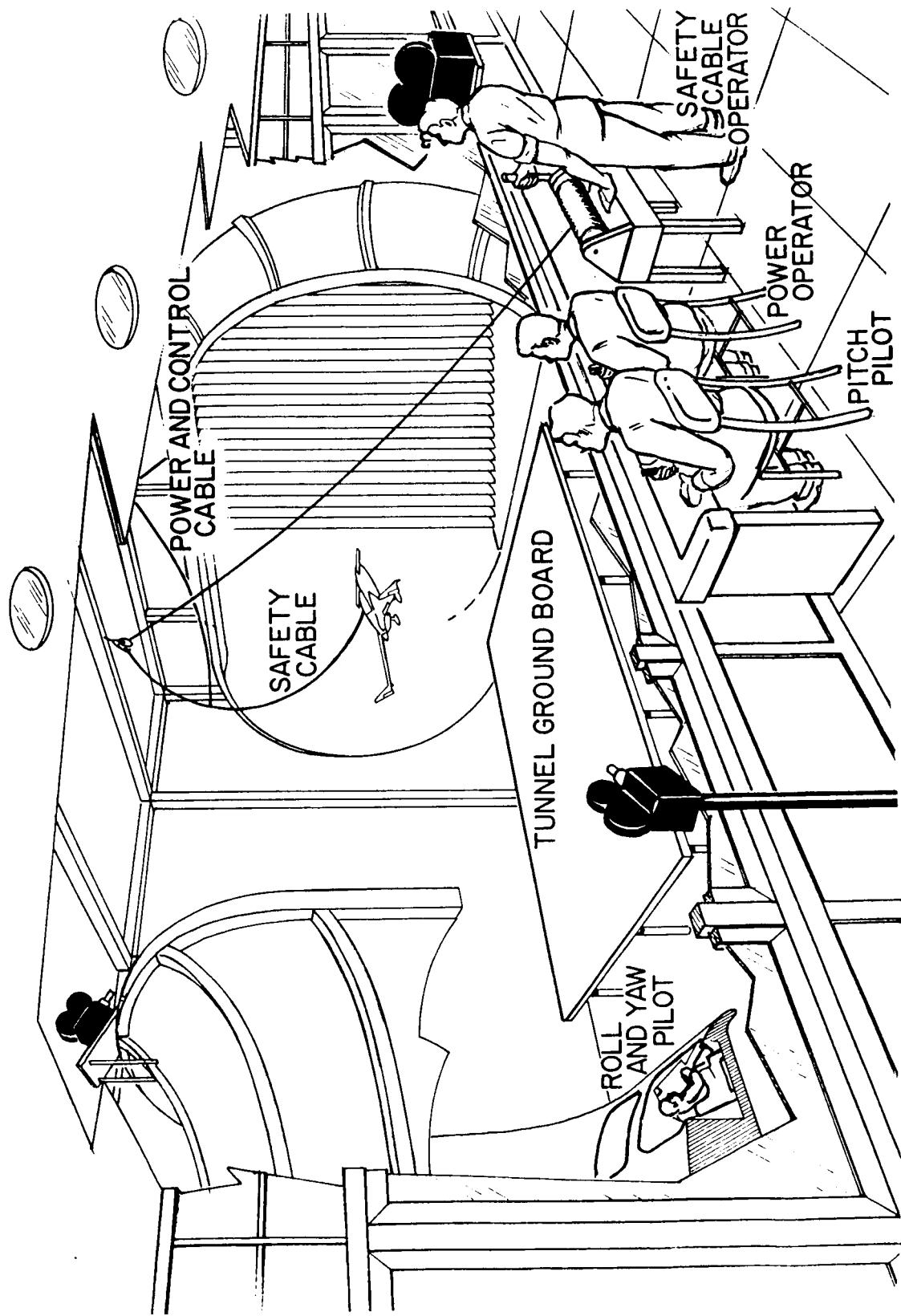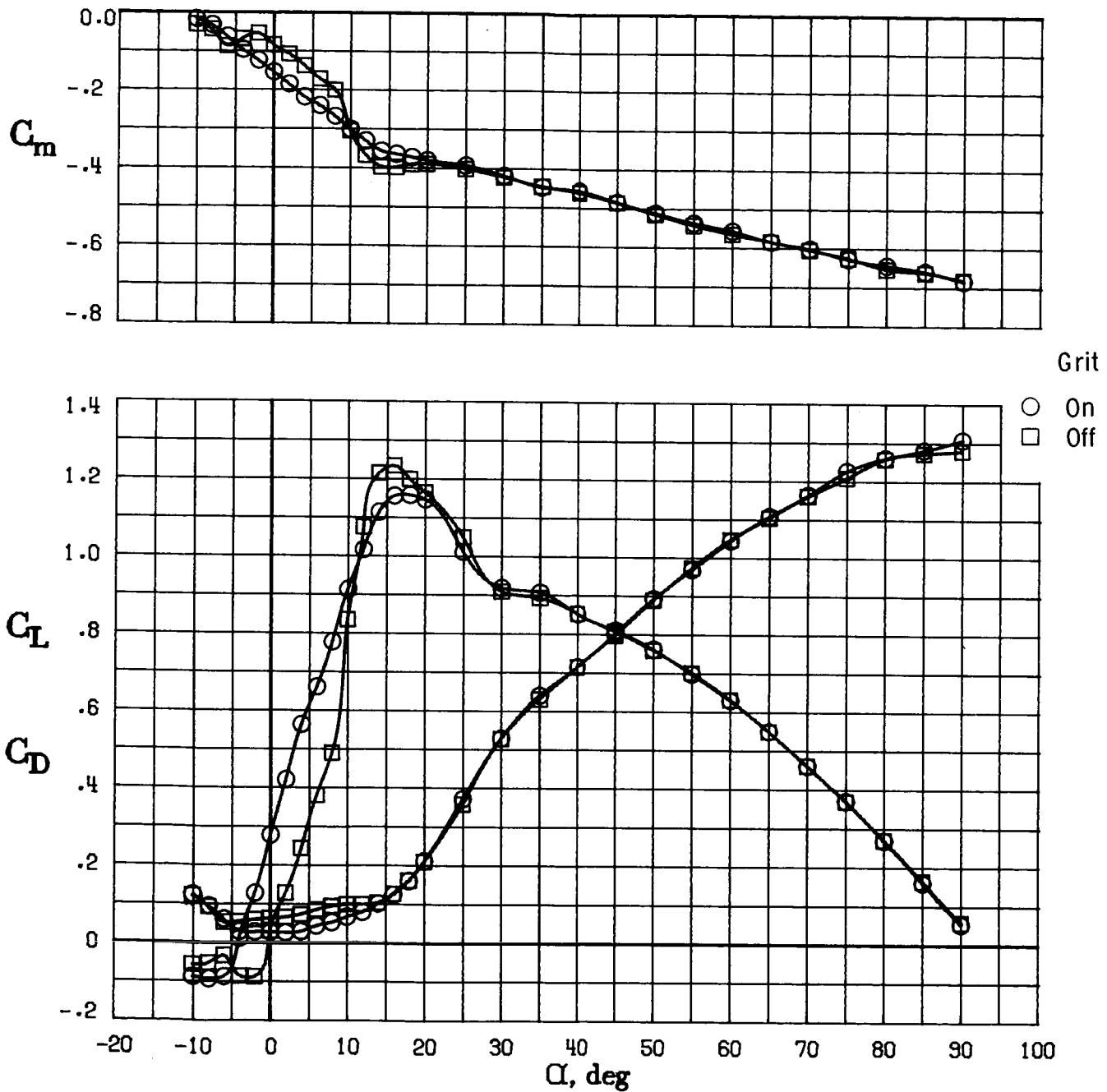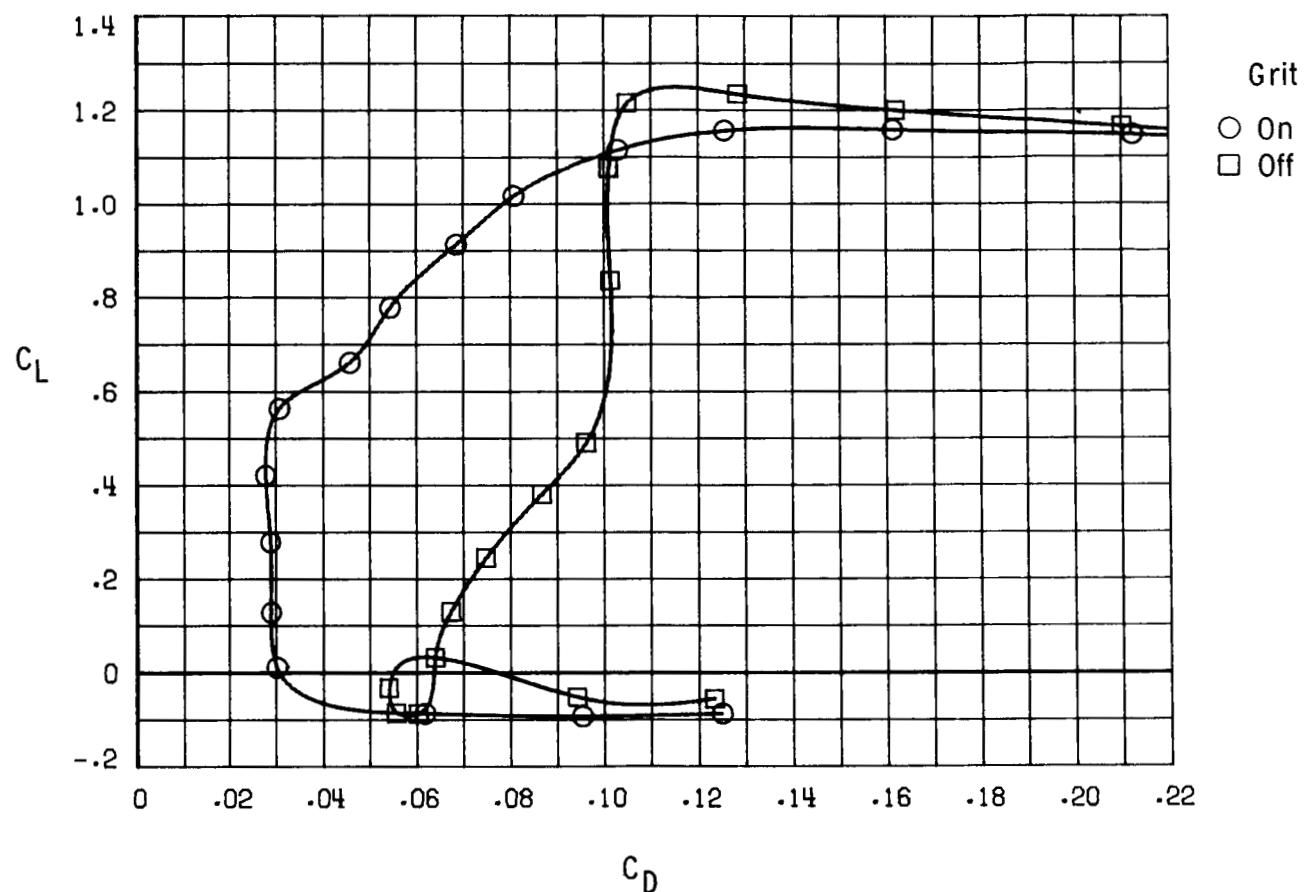
Figure 7. Free-flight test setup.

SAFETY CABLE OPERATOR

POWER OPERATOR

PITCH PILOT

POWER AND CONTROL CABLE

SAFETY CABLE

TUNNEL GROUND BOARD

ROLL AND YAW PILOT

(a) Lift and drag characteristics of canard alone.

Figure 8. Transition grit effects on canard aerodynamics. Referenced to canard area; high canard position; $\delta_e = 0°$; $i_c = 0°$.

(b) Drag characteristics of canard alone.

Figure 8. Concluded.
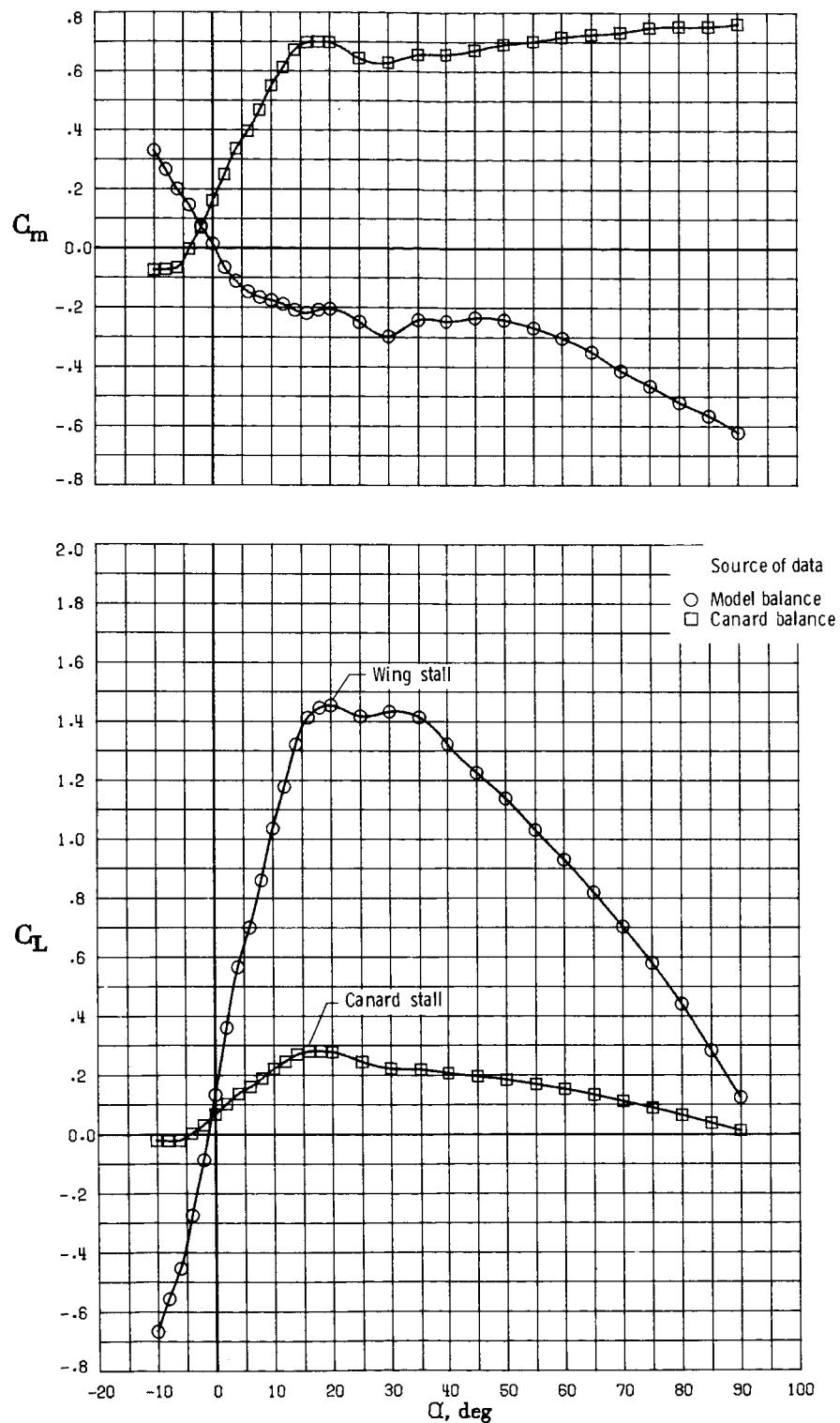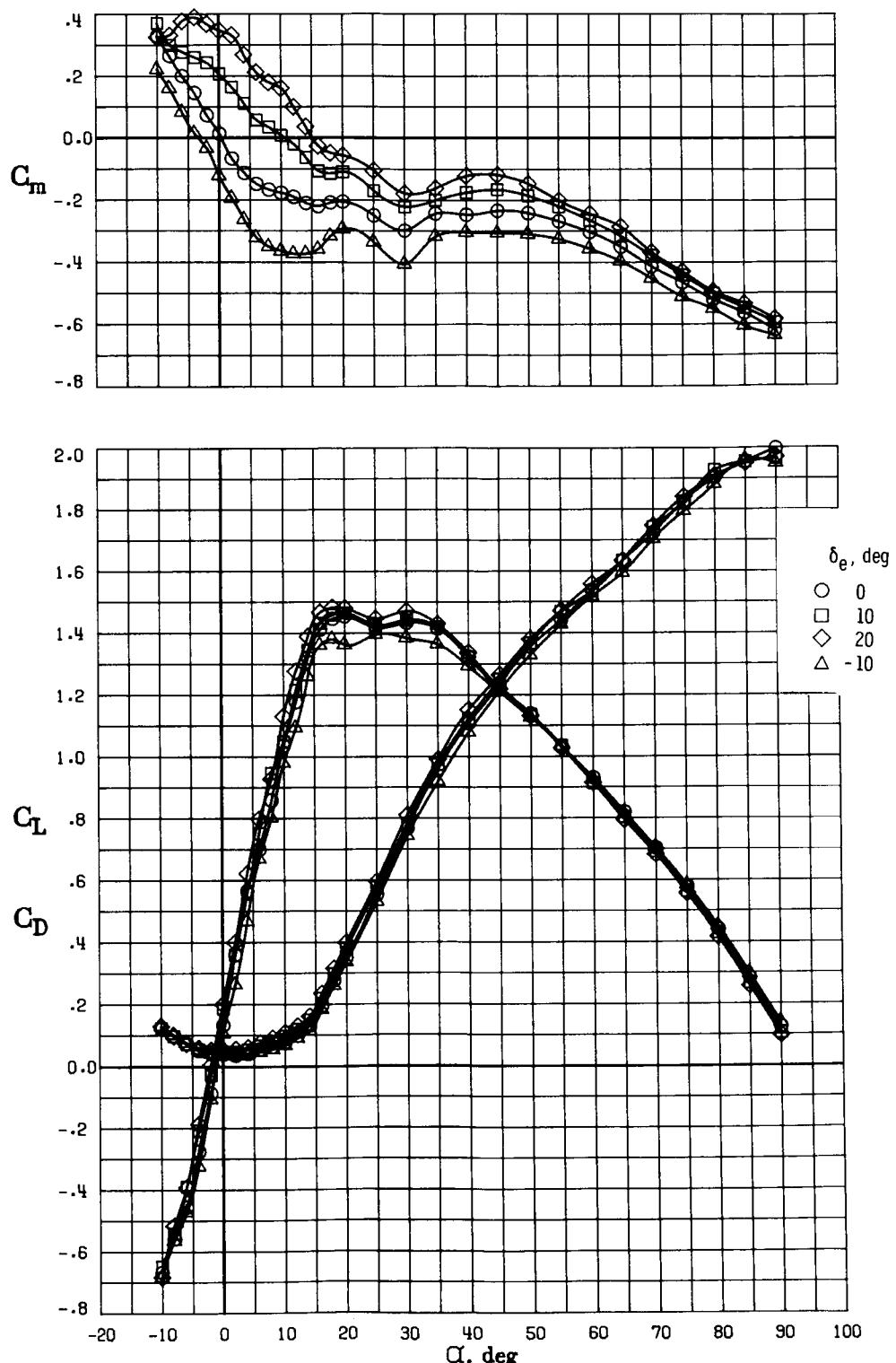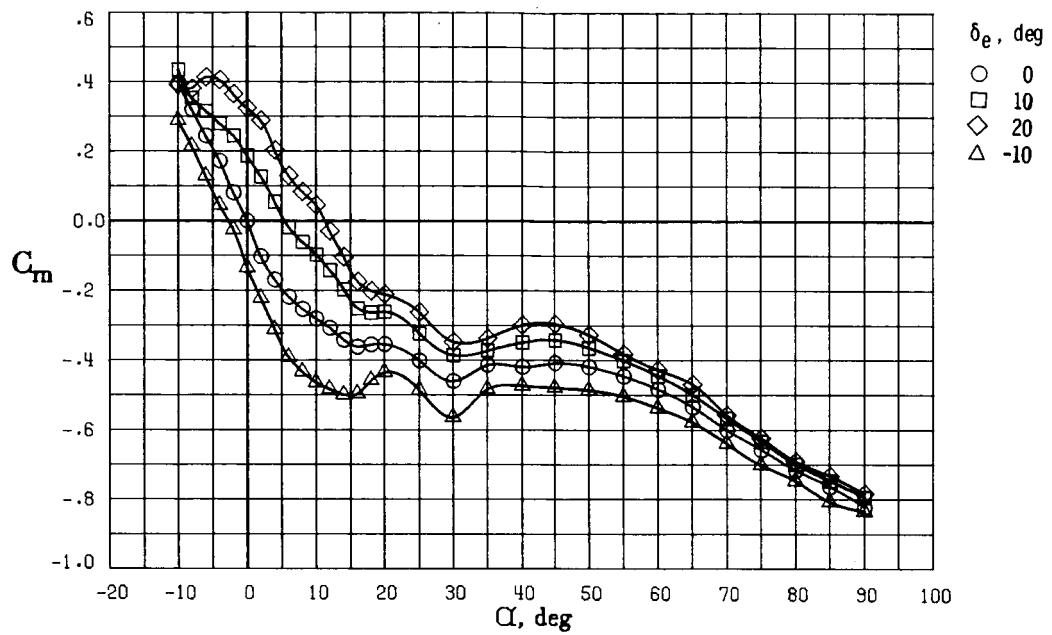
Figure 9. Canard contribution to model lift and pitching-moment characteristics. High canard position; $\delta_e = 0°$; $i_c = 0°$.
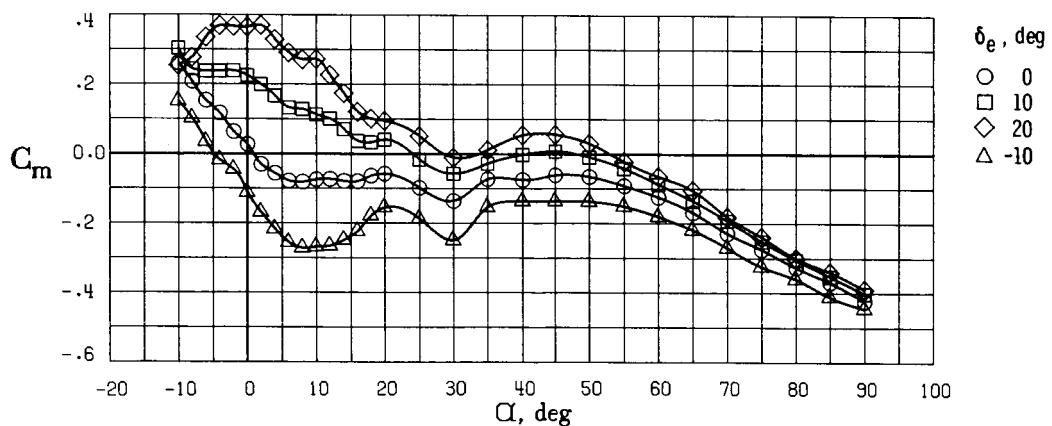
(a) Mid c.g. position.

Figure 10. Elevator effectiveness of the basic configuration. High canard position; $i_c = 0°$.
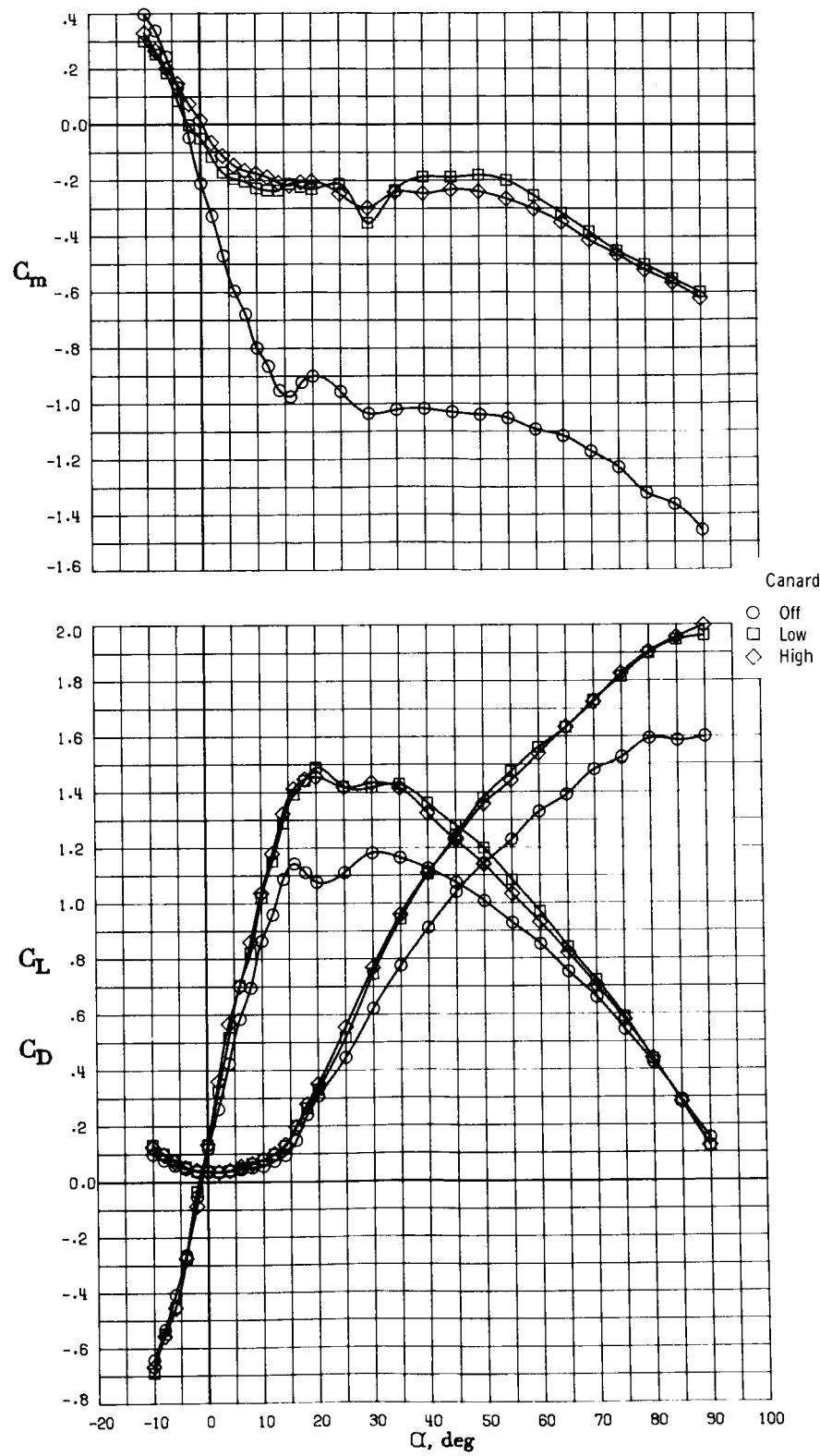
(b) Forward c.g. position.
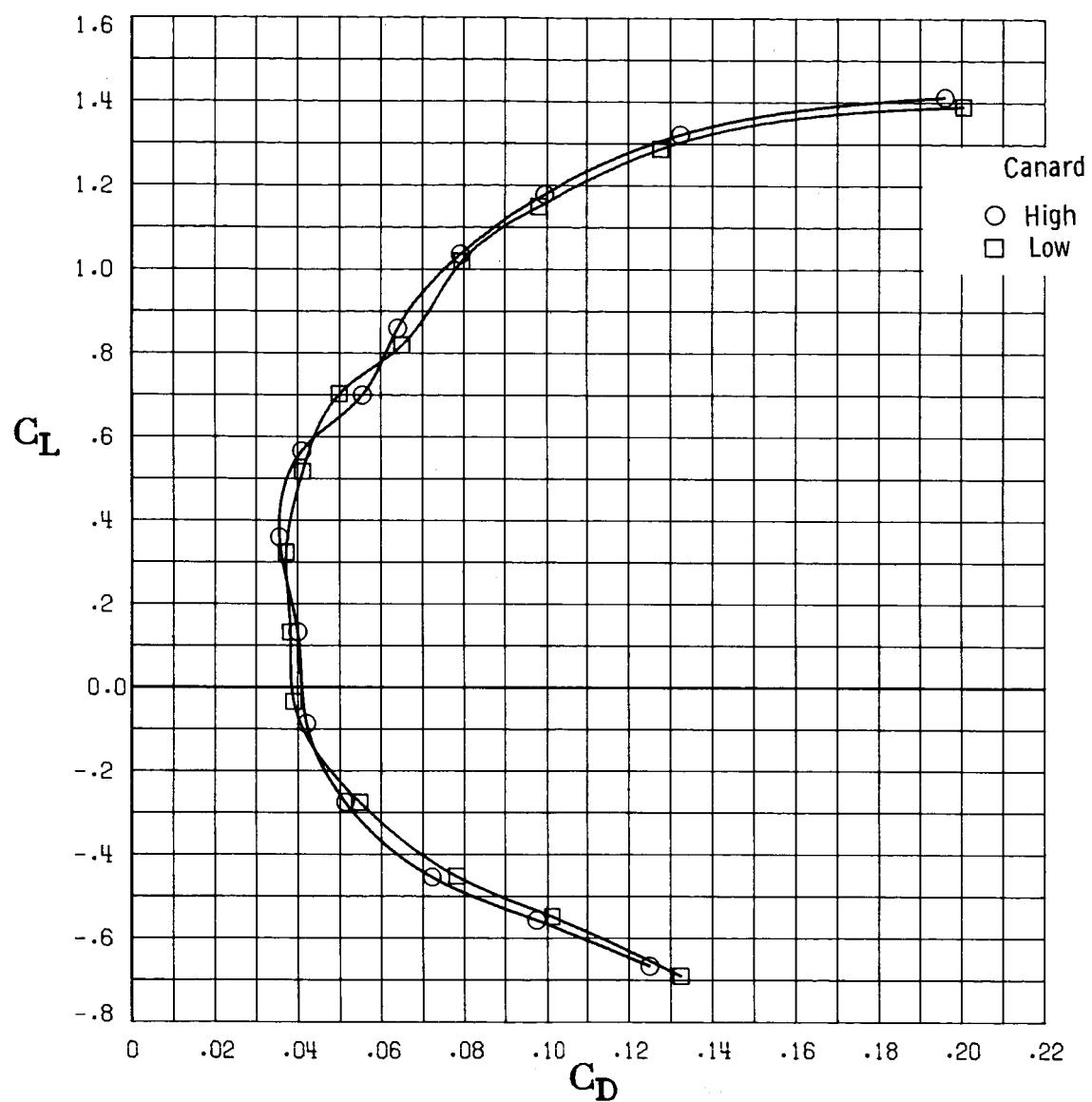
(c) Aft c.g. position.

Figure 10. Concluded.

(a) Lift and pitching-moment characteristics.

Figure 11. Canard position effects on longitudinal aerodynamics. $\delta_e = 0°$; $i_c = 0°$.

(b) Drag characteristics.

Figure 11. Concluded.
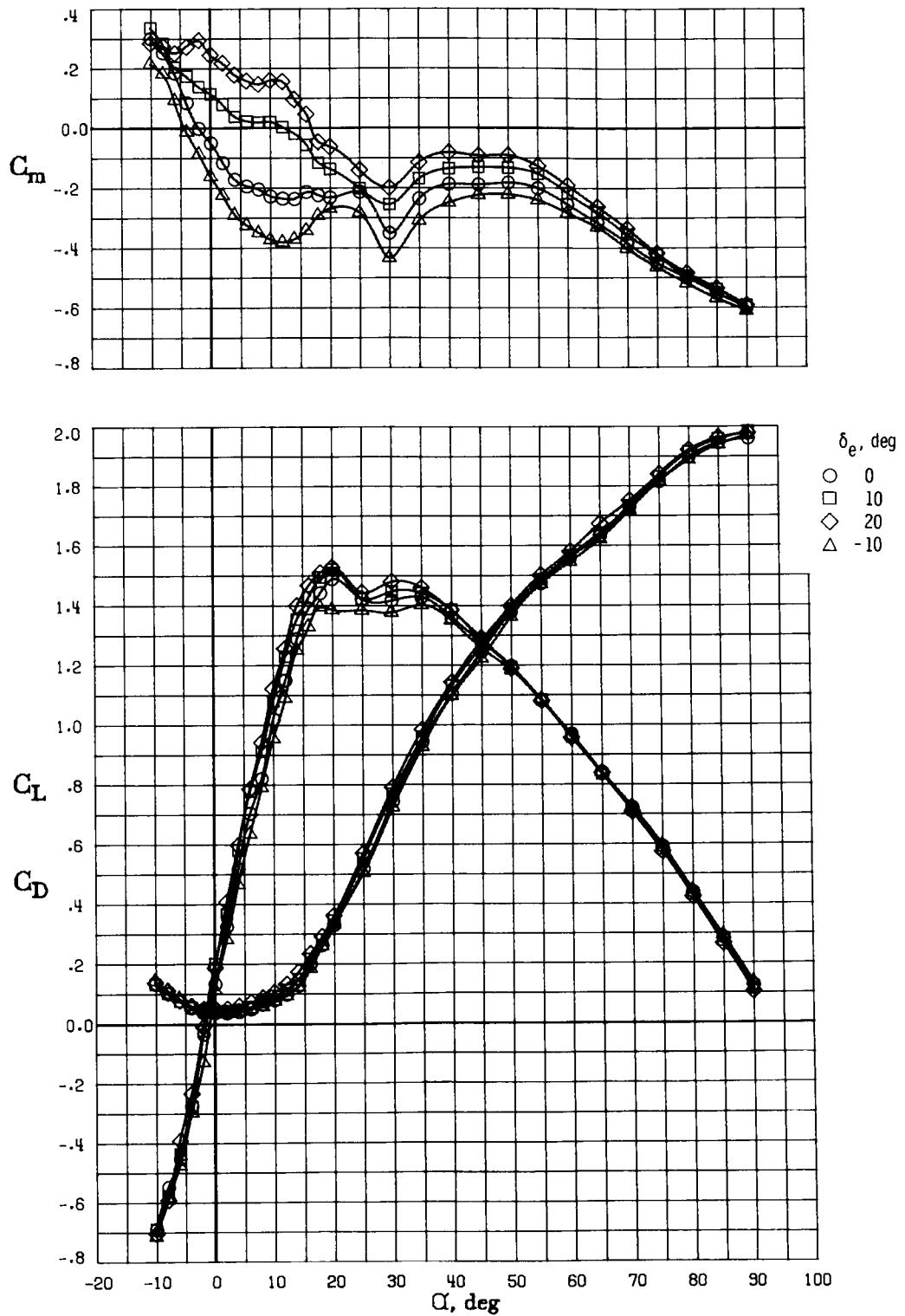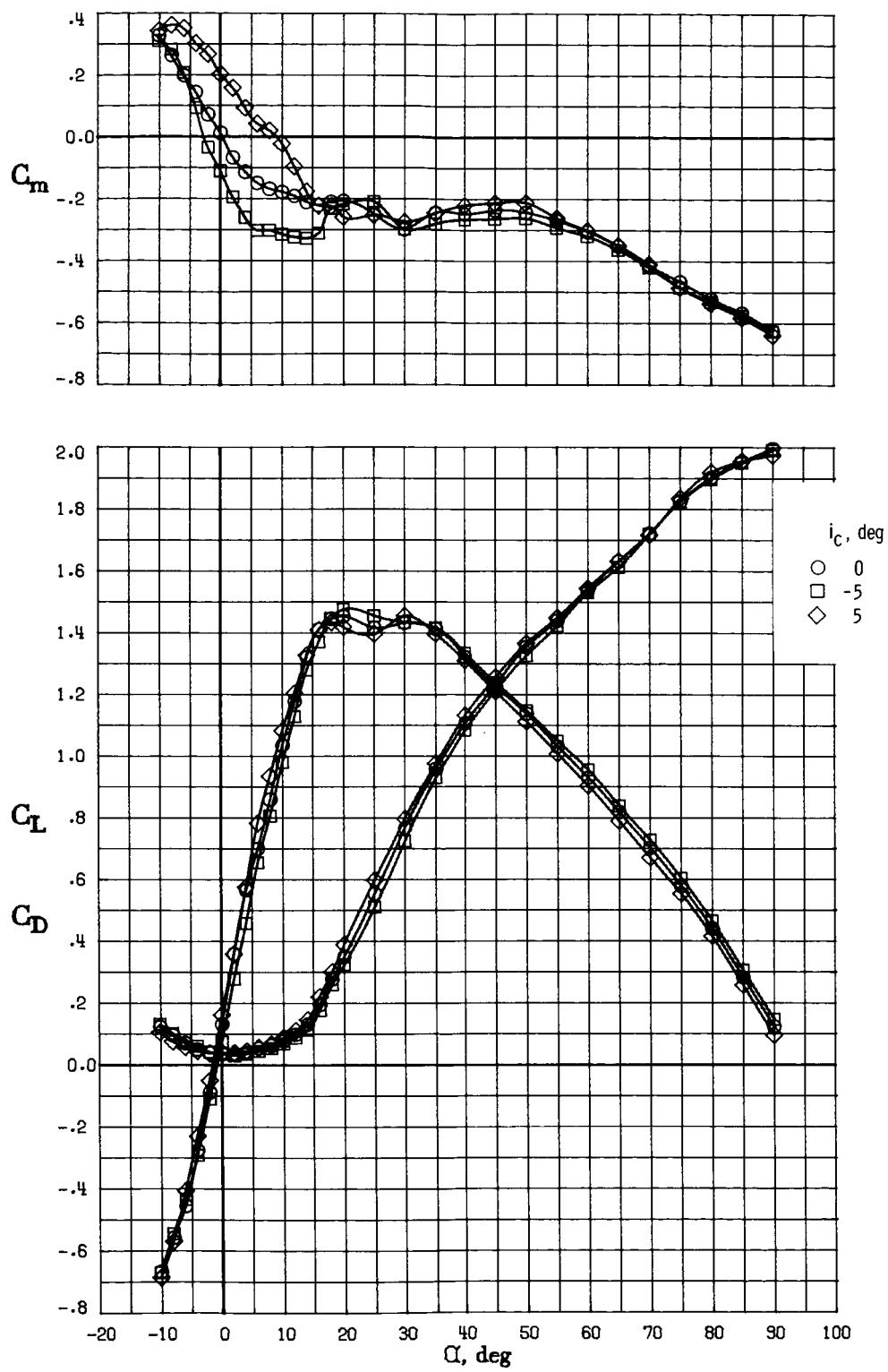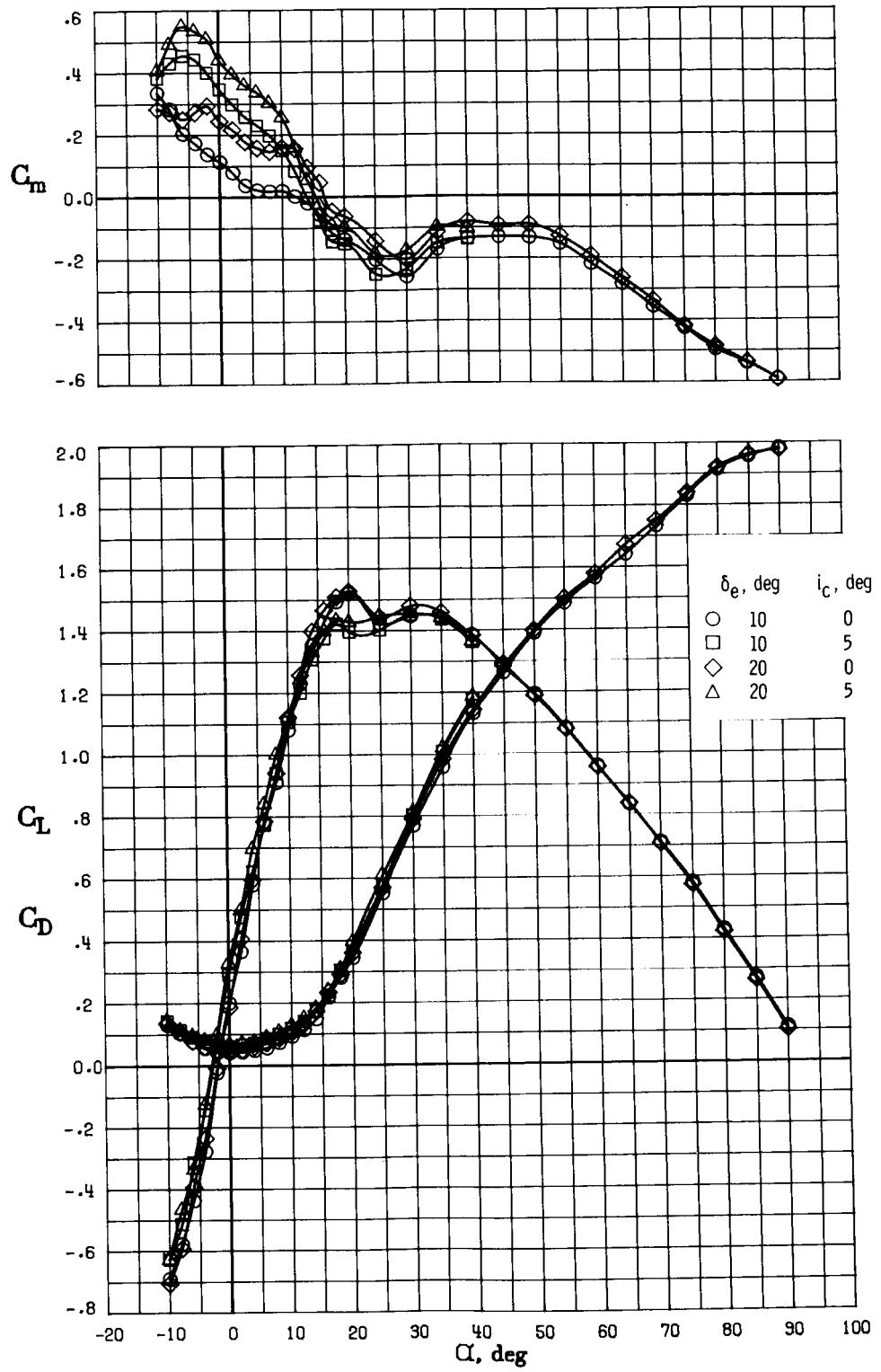
Figure 12. Elevator effectiveness with low canard position. $i_c = 0°$.

(a) High canard position; $\delta_e = 0°$.

Figure 13. Canard incidence effects on lift and pitching-moment characteristics.

(b) Low canard position.

Figure 13. Concluded.
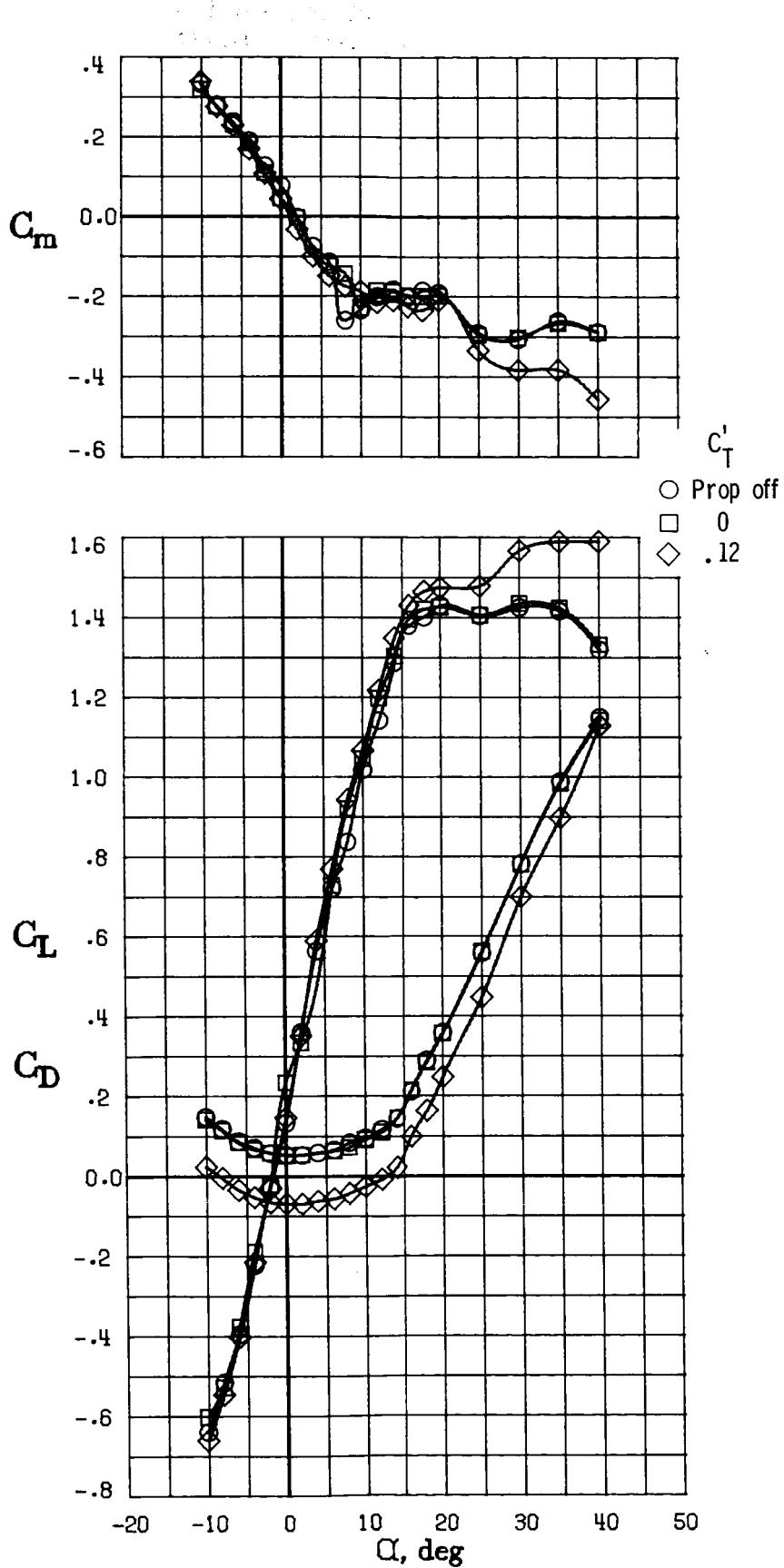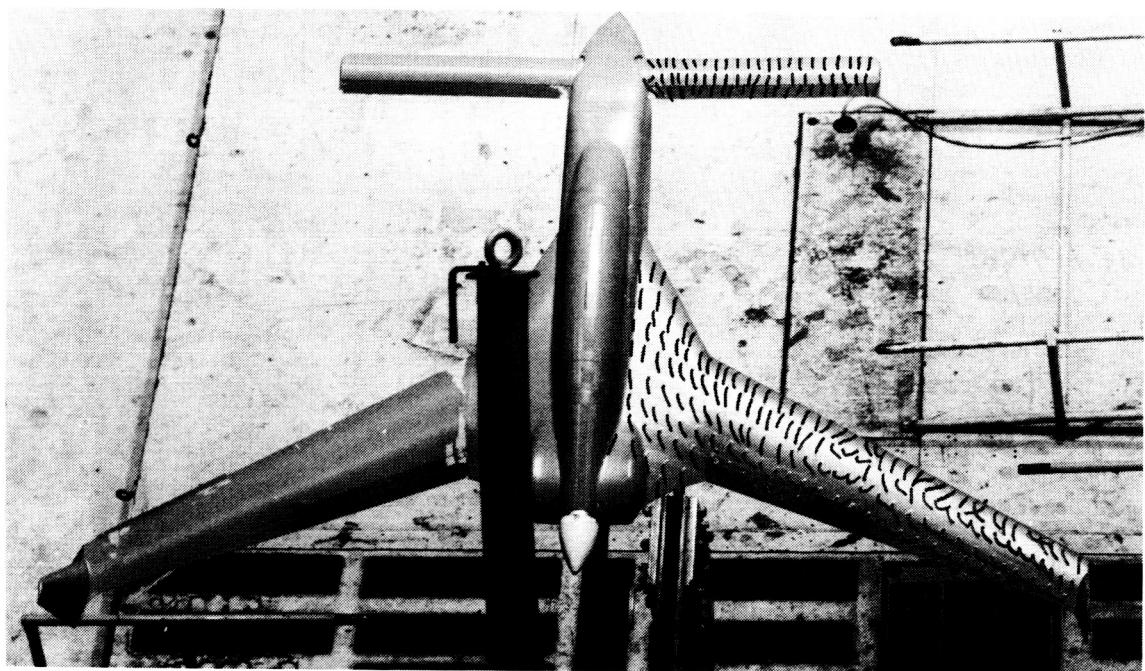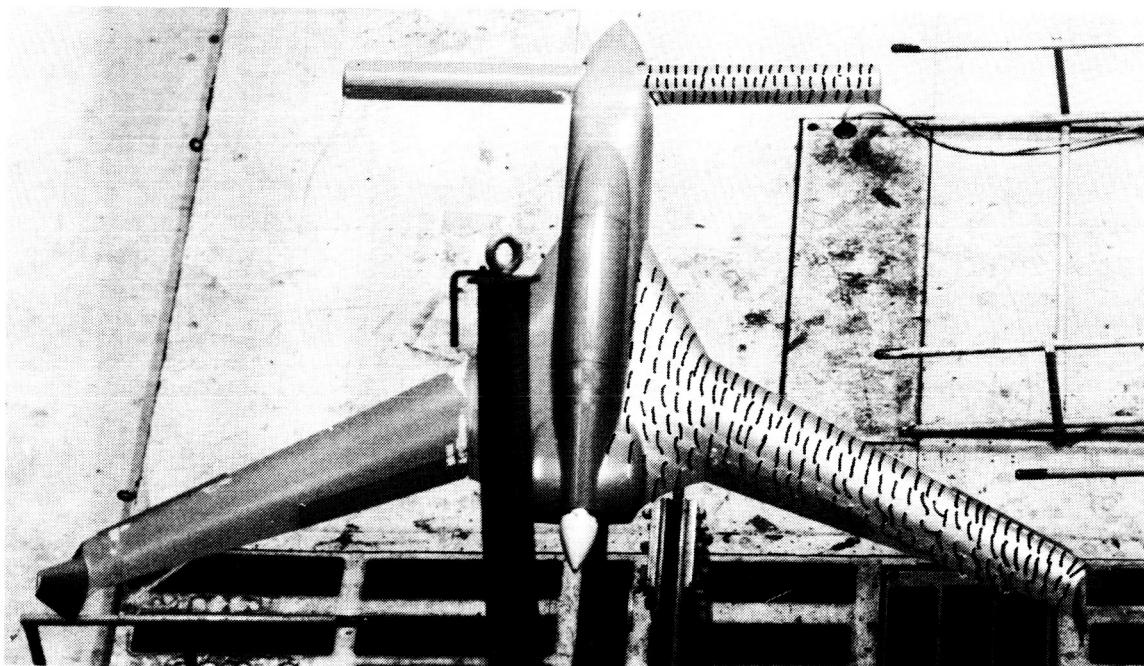
Figure 14. Thrust effects on lift and pitching-moment characteristics. High canard position; $\delta_e = 0°$; $i_c = 0°$.
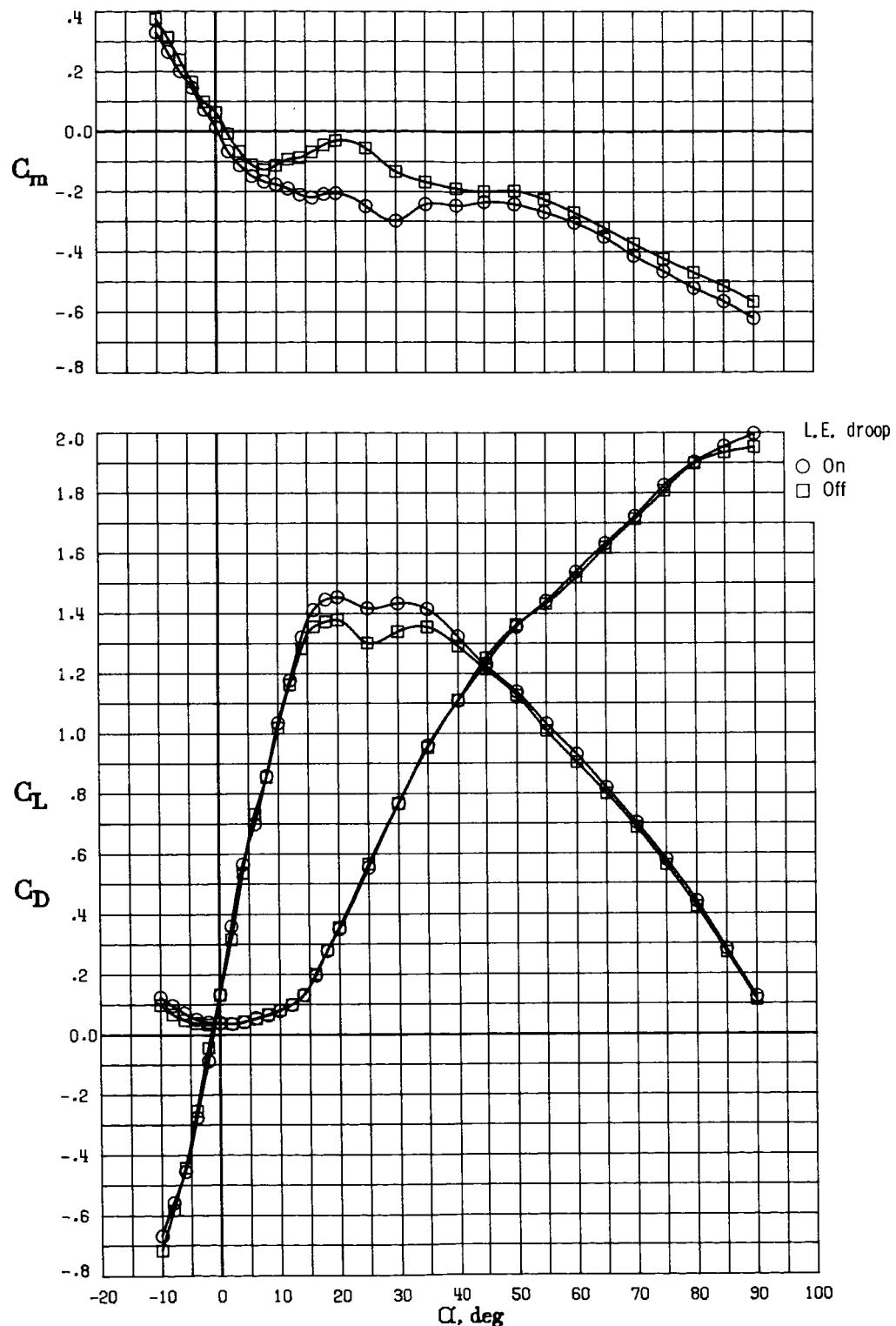
(a) Leading-edge droop removed.

L-86-347
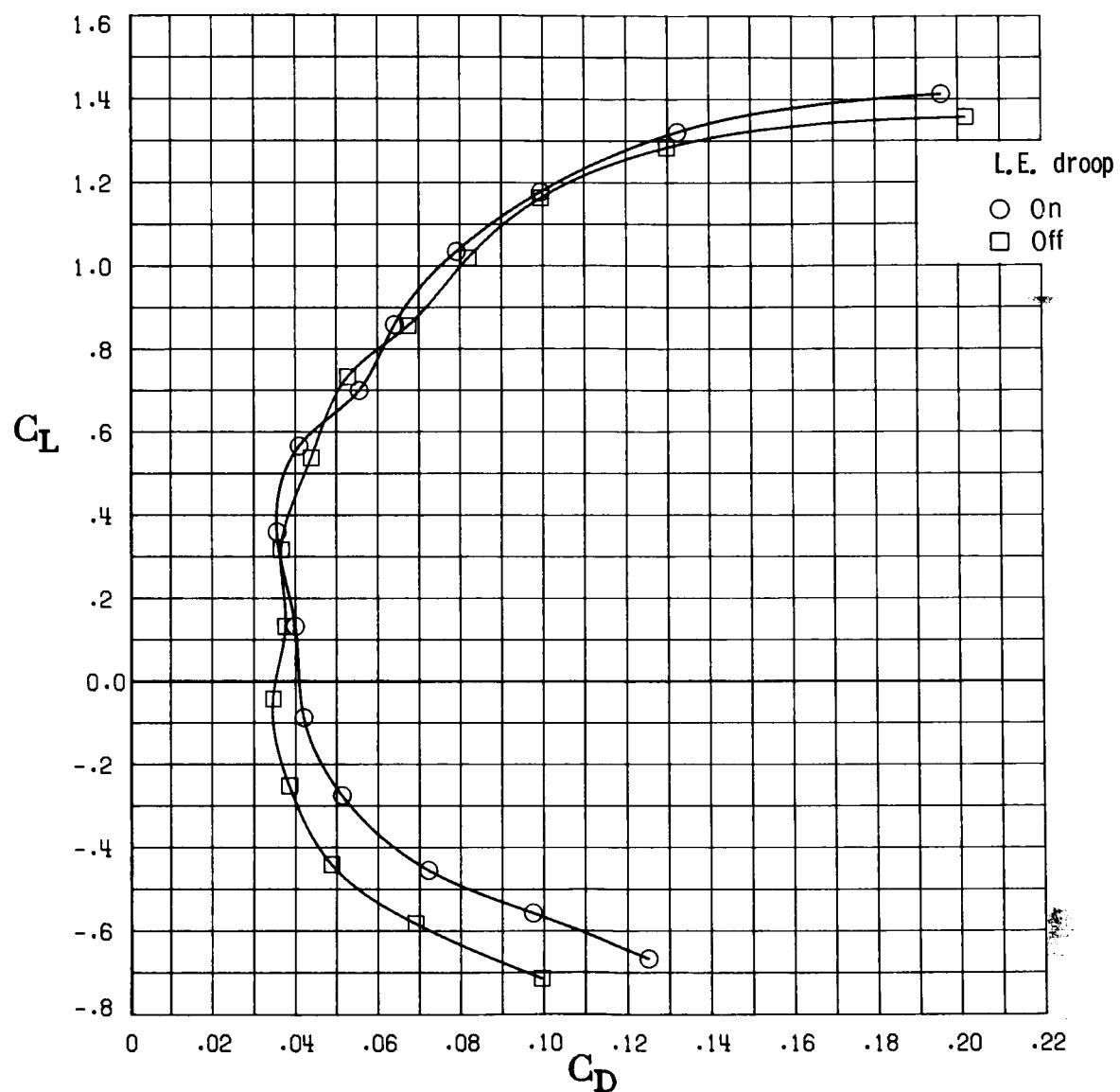
(b) Leading-edge droop installed.

Figure 15. Tuft studies of stall characteristics of wing. $\alpha = 16°$.

(a) Lift and pitching-moment characteristics.

Figure 16. Effect of leading-edge droop on longitudinal characteristics. High canard position; $\delta_e = 0°$; $i_c = 0°$.

(b) Drag characteristics.

Figure 16. Concluded.
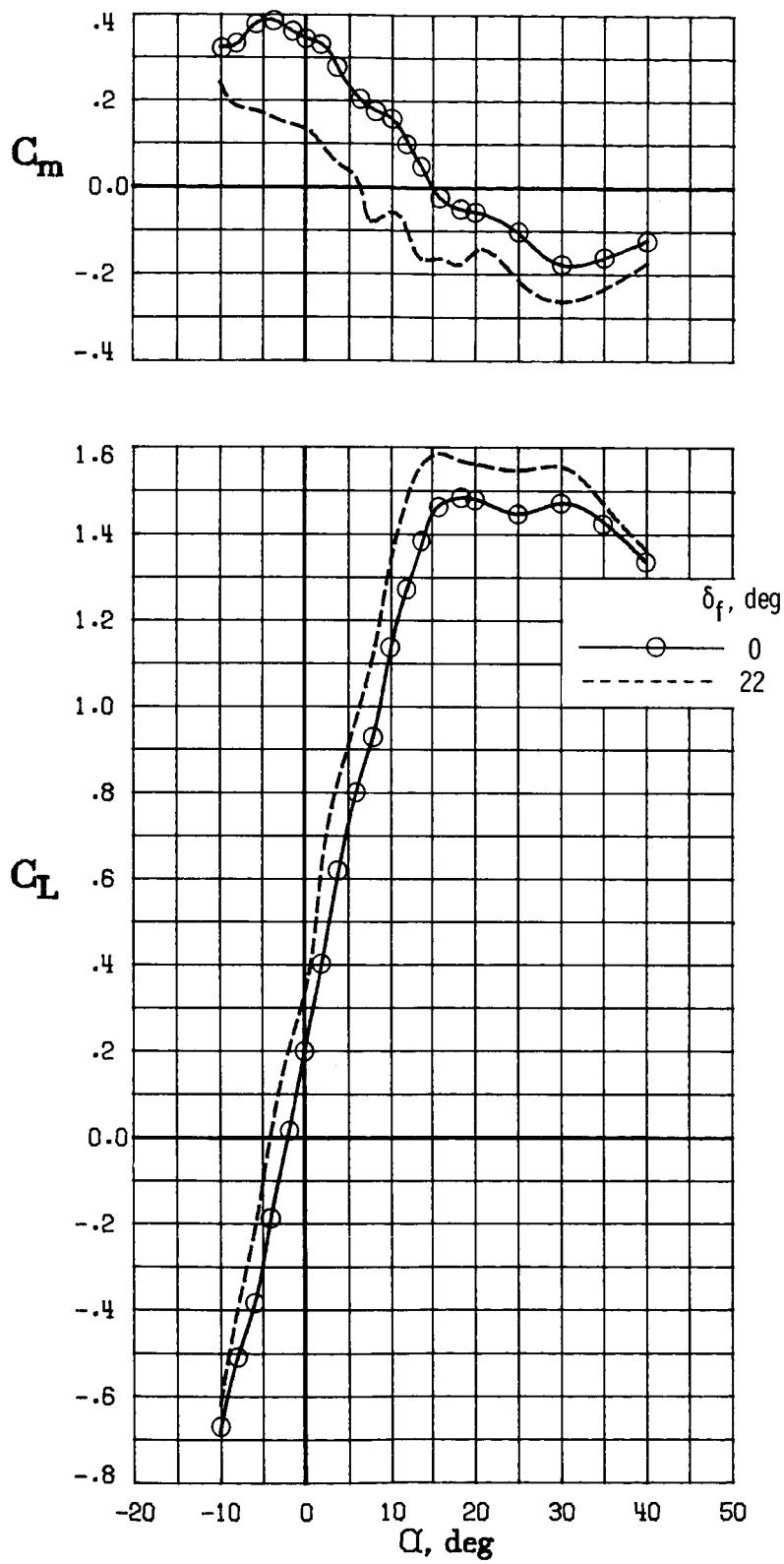
Figure 17. Landing flap effects on lift and pitching-moment characteristics. High canard position; $\delta_e = 20°$; $i_c = 0°$.
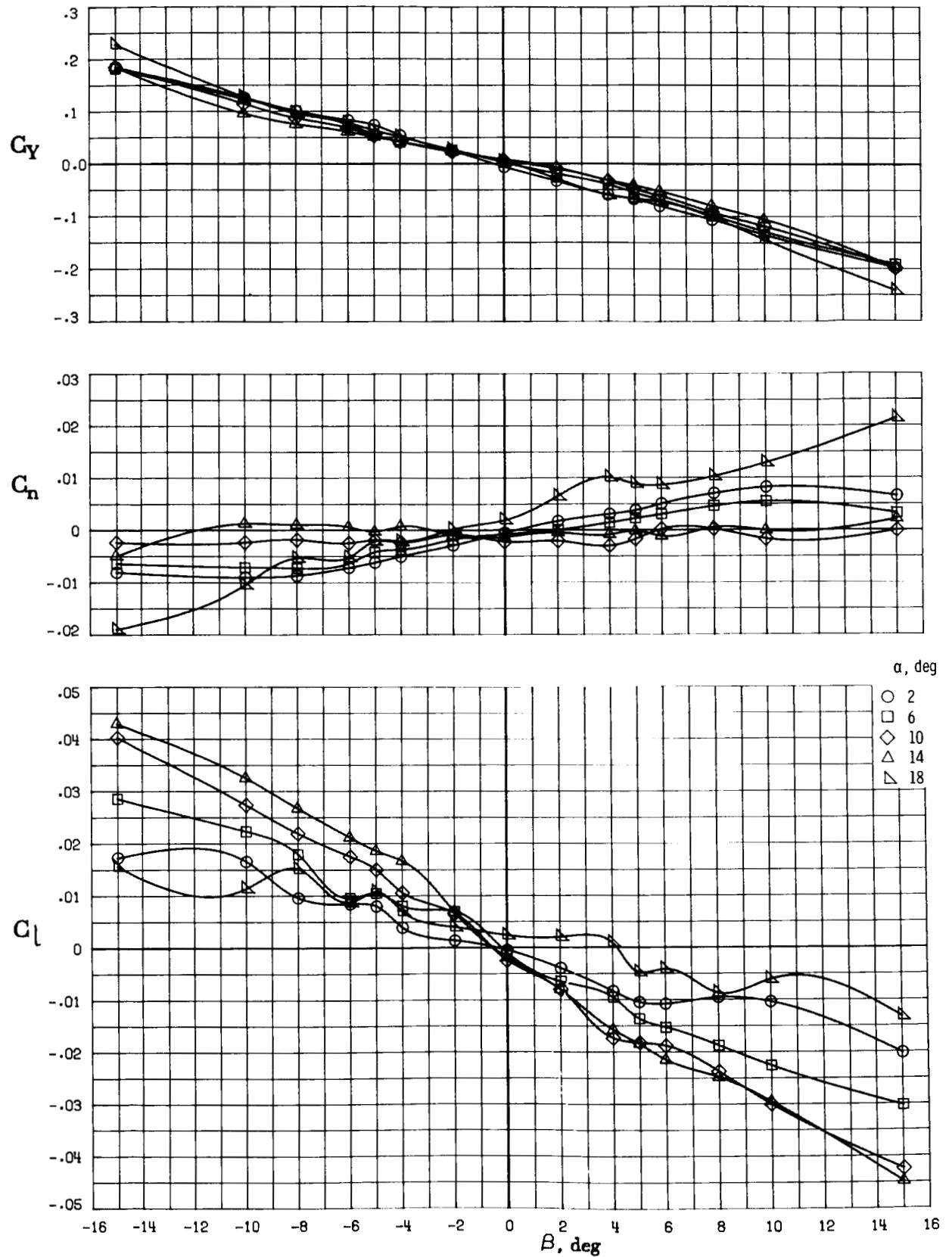
Figure 18. Lateral-directional characteristics of configuration in sideslip. High canard position; $\delta_e = 0°$; $i_c = 0°$.
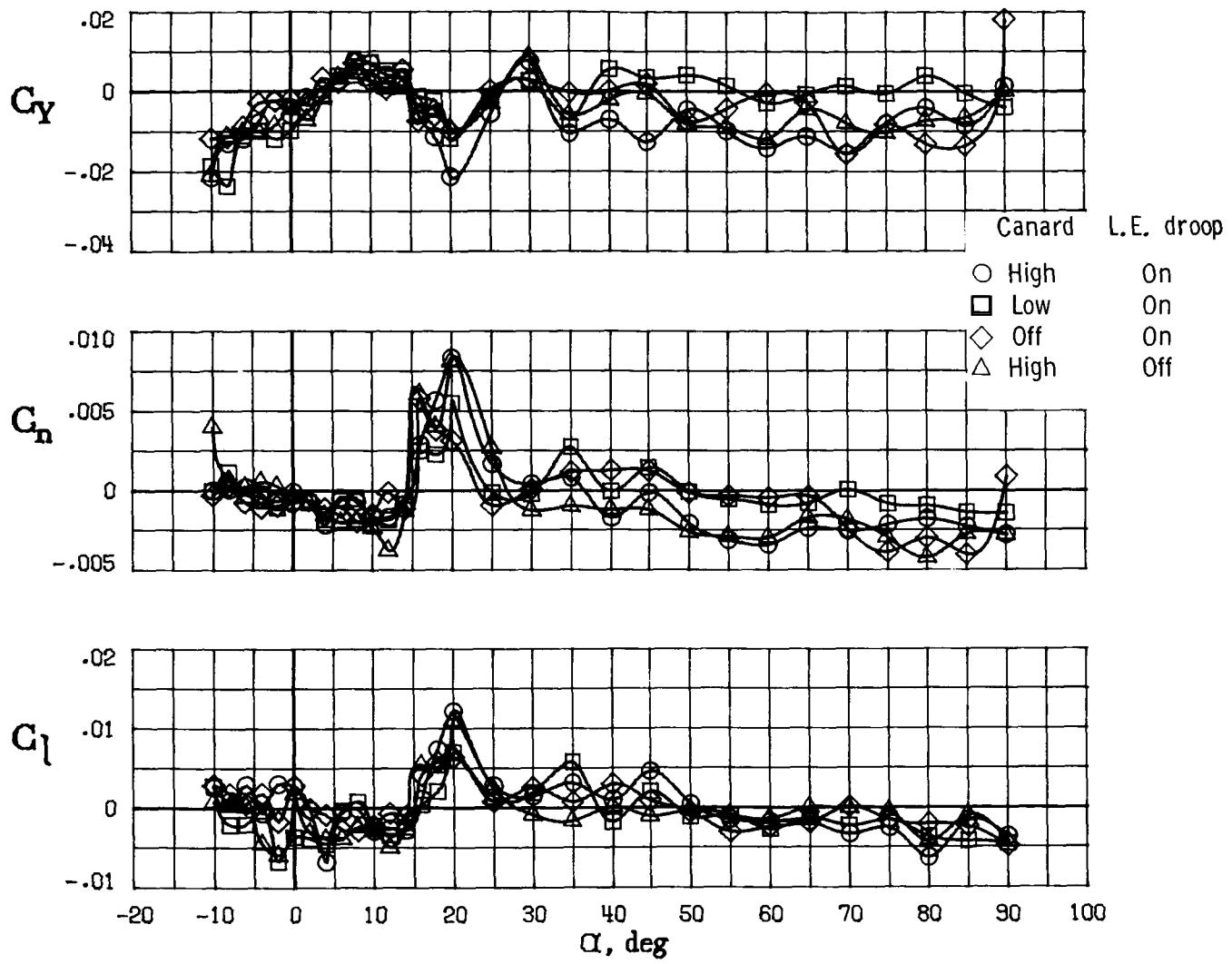
Figure 19. Canard and leading-edge droop effects on lateral-directional characteristics. $\beta = 0°$; $\delta_e = 0°$; $i_c = 0°$.
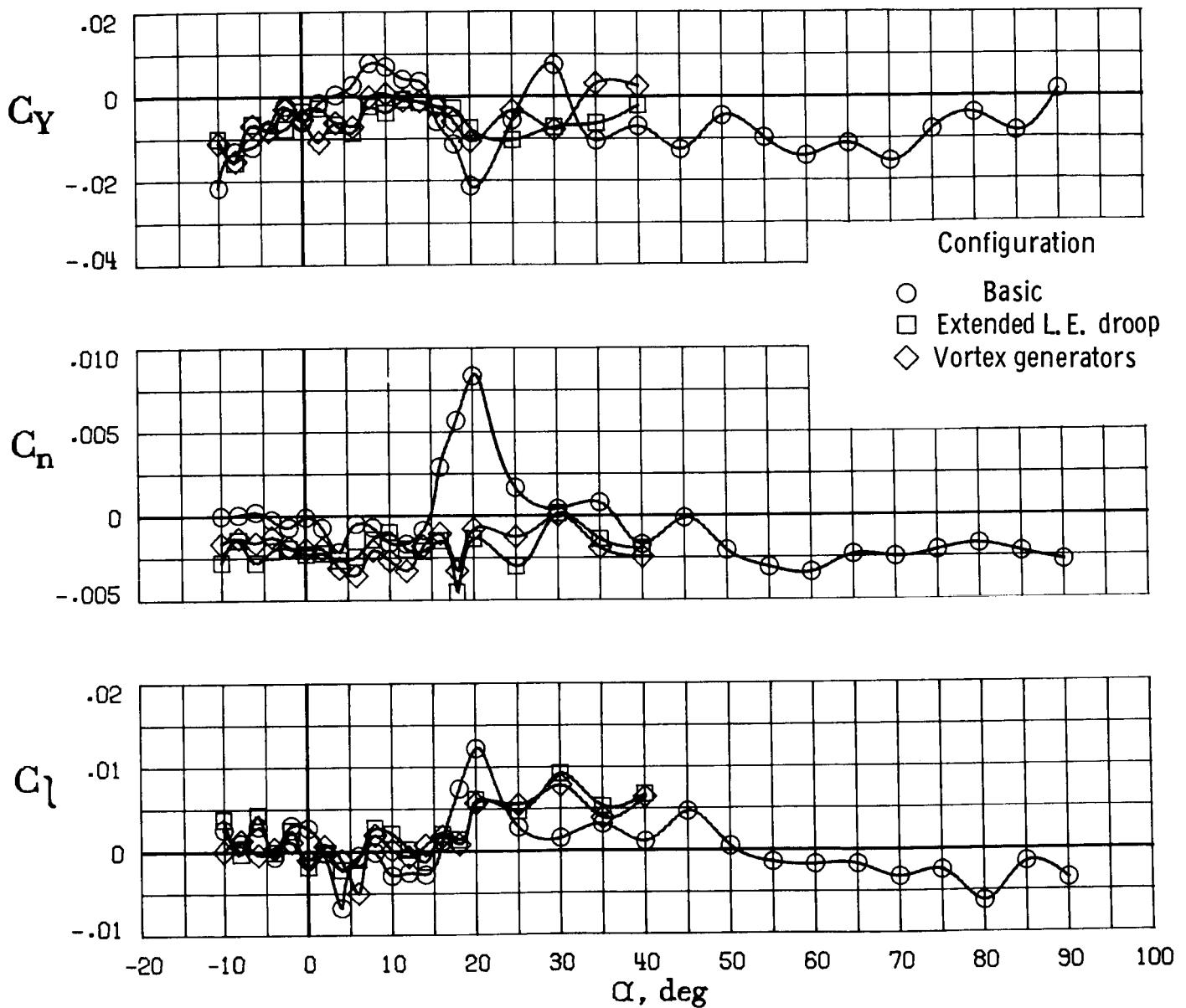
Figure 20. Effect of installation of vortex generators and extended leading-edge droop on lateral-directional characteristics. $\beta = 0°$; high canard position; $\delta_e = 0°$; $i_c = 0°$.
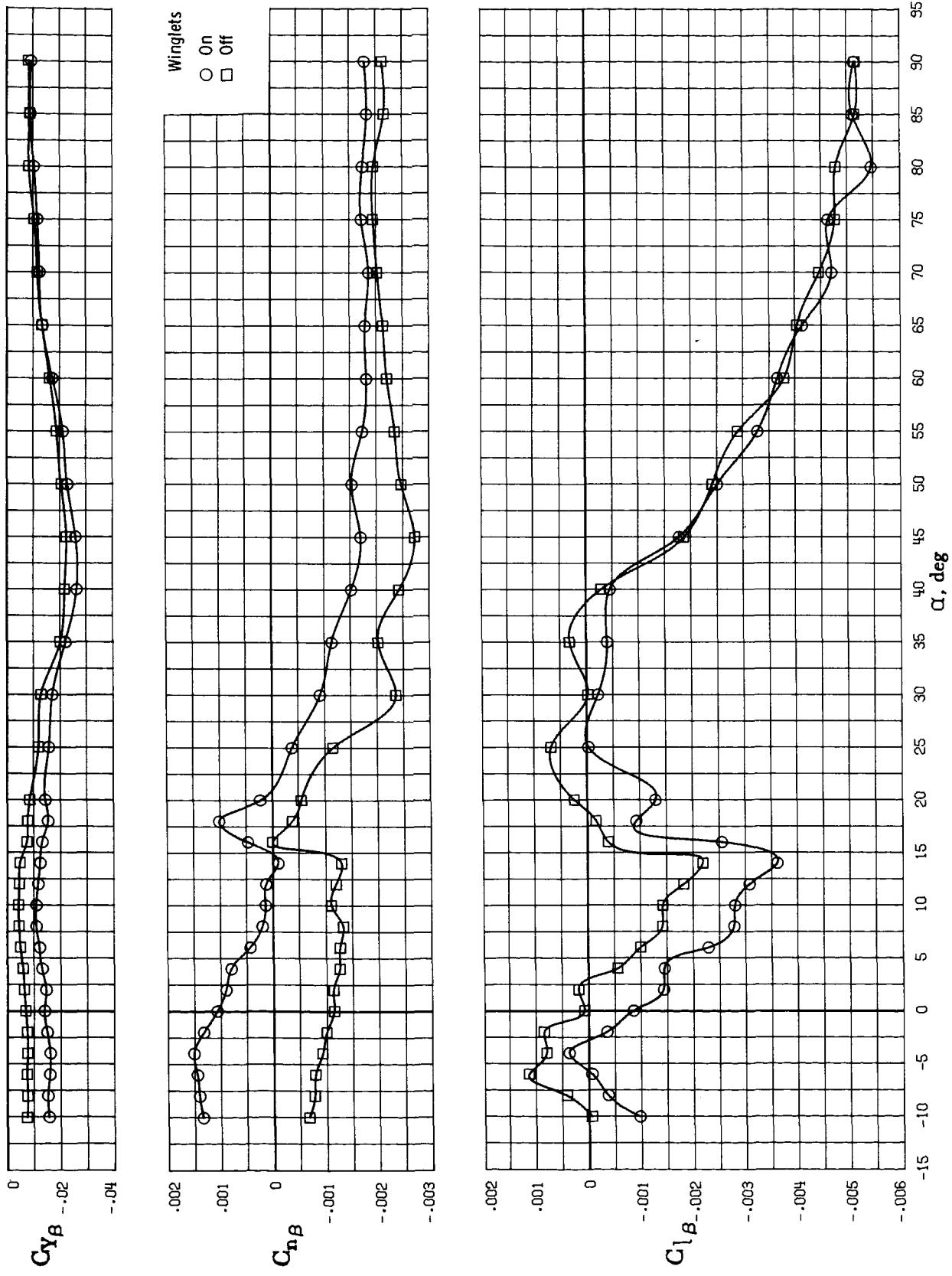
Figure 21. Winglet effects on lateral-directional static stability. High canard position; $\delta_e = 0°$; $i_c = 0°$.
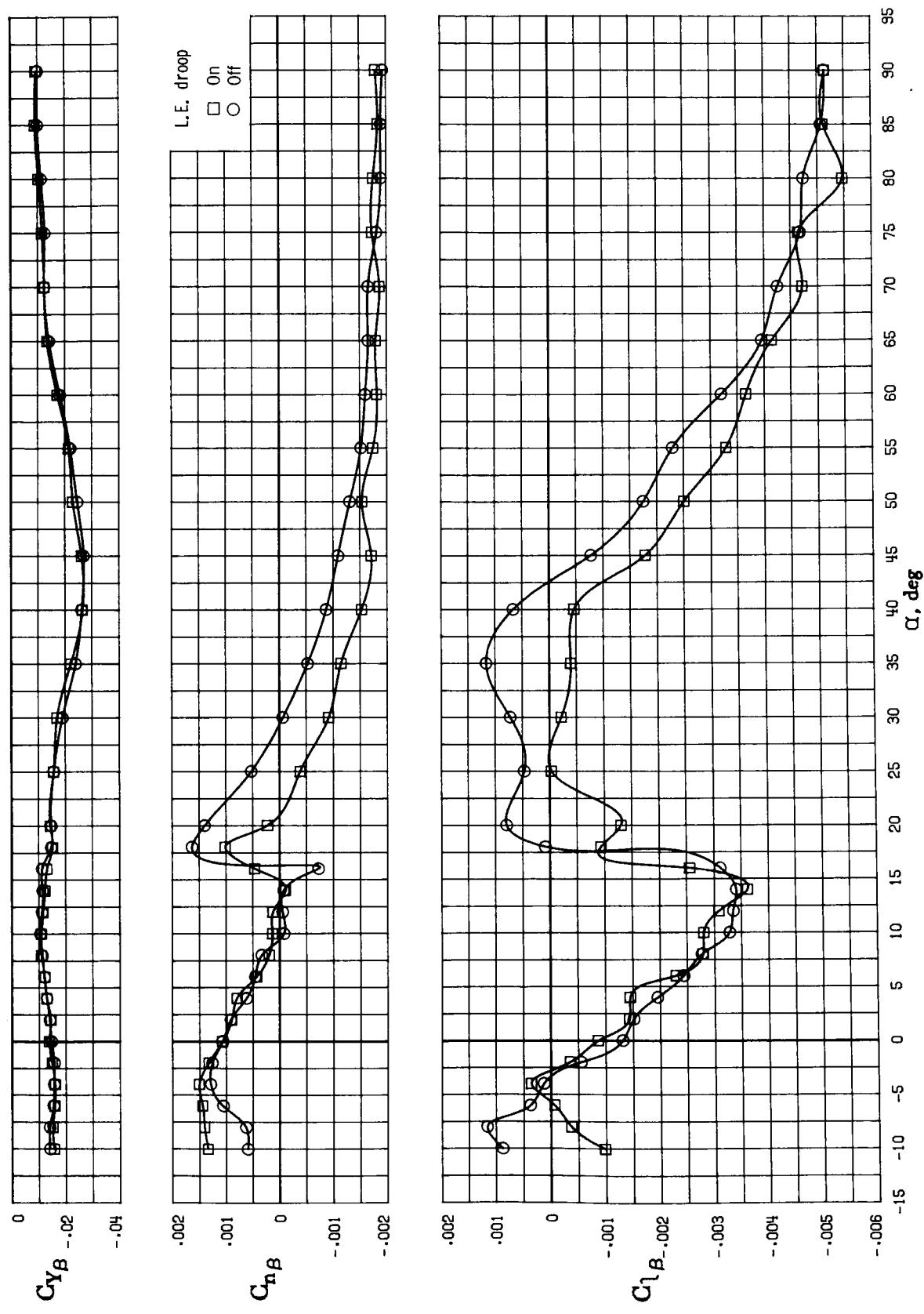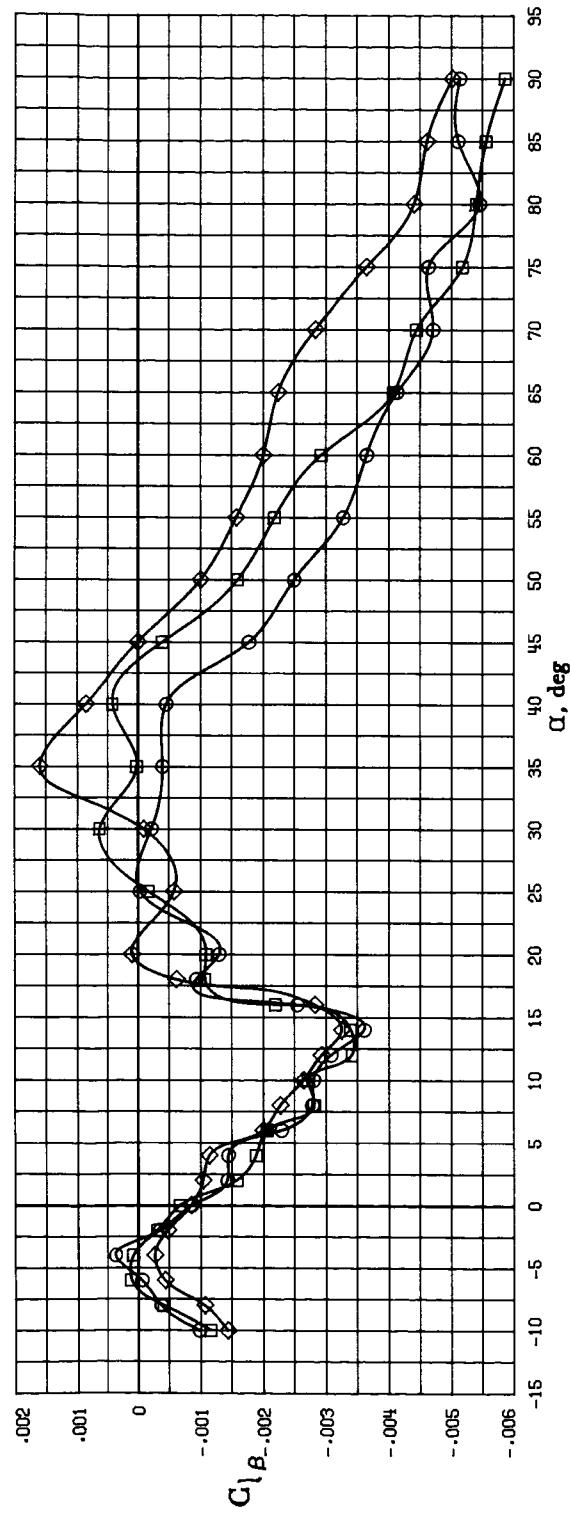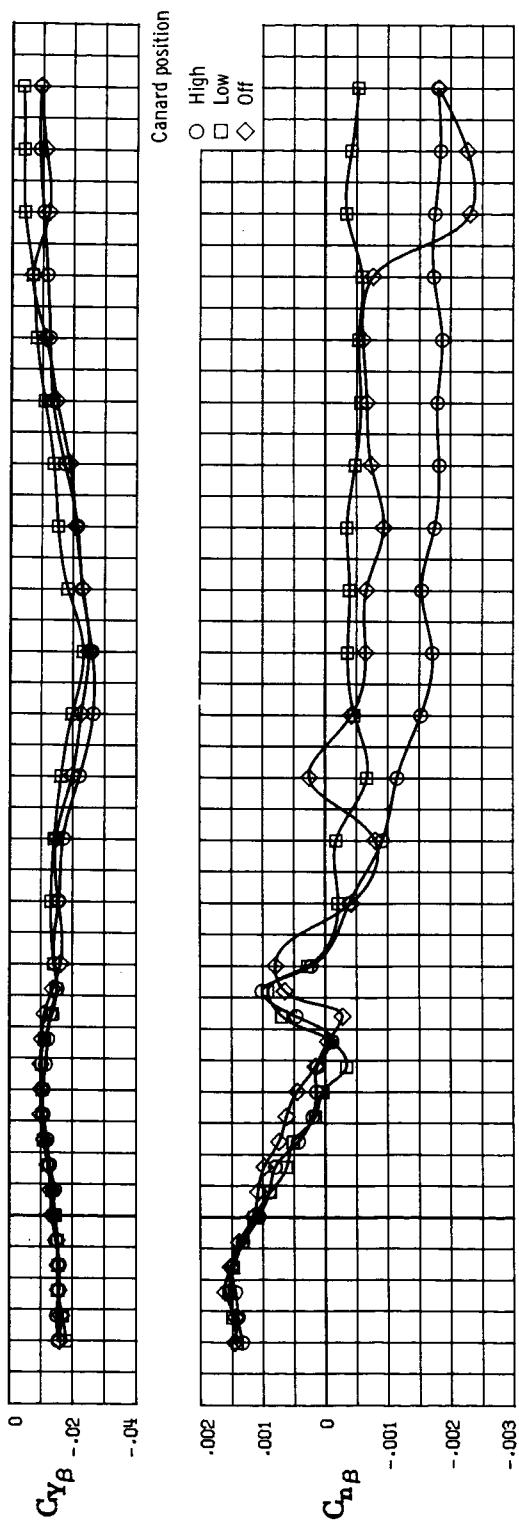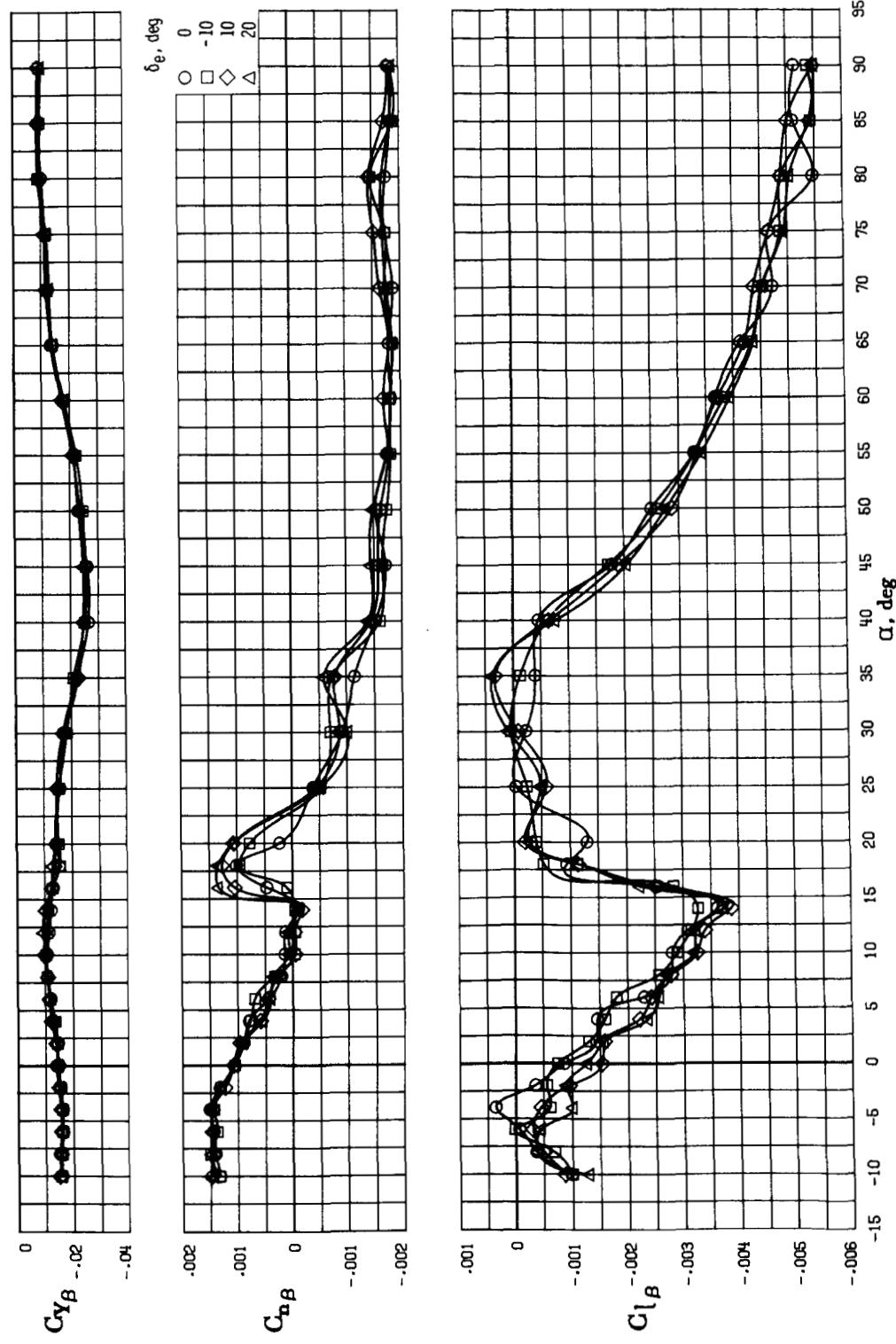
Figure 22. Leading-edge droop effects on lateral-directional static stability. High canard position; $\delta_e = 0°$; $i_c = 0°$.

(a) Effect of canard position; $\delta_e = 0°$.

Figure 23. Effect of canard on lateral-directional static stability. $i_c = 0°$.

(b) Effect of elevator deflection; high canard position.

Figure 23. Concluded.
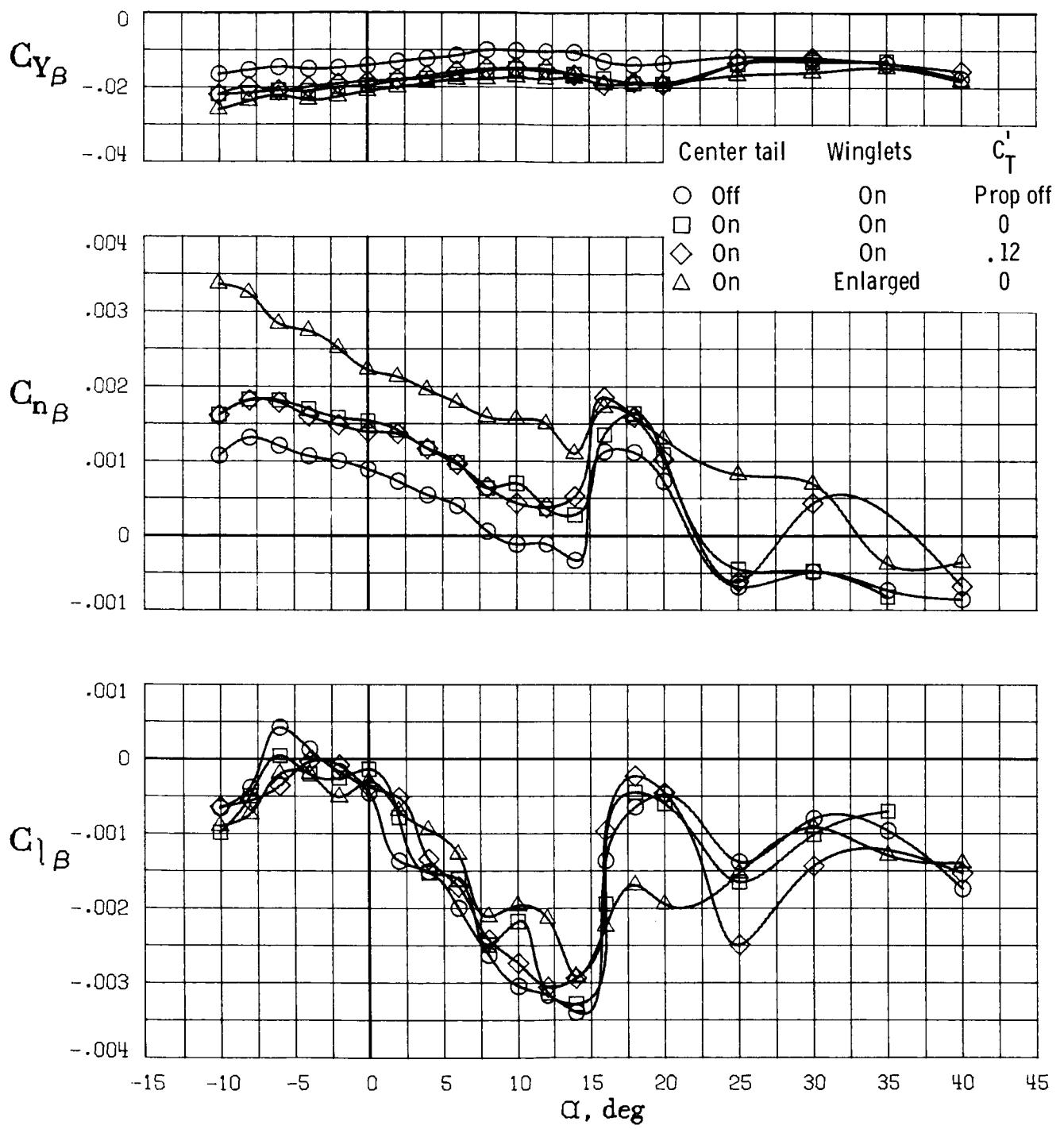
Figure 24. Effect of center vertical tail and enlarged winglets on lateral-directional static stability. Low canard position; $\delta_e = 0°$; $i_c = 0°$.
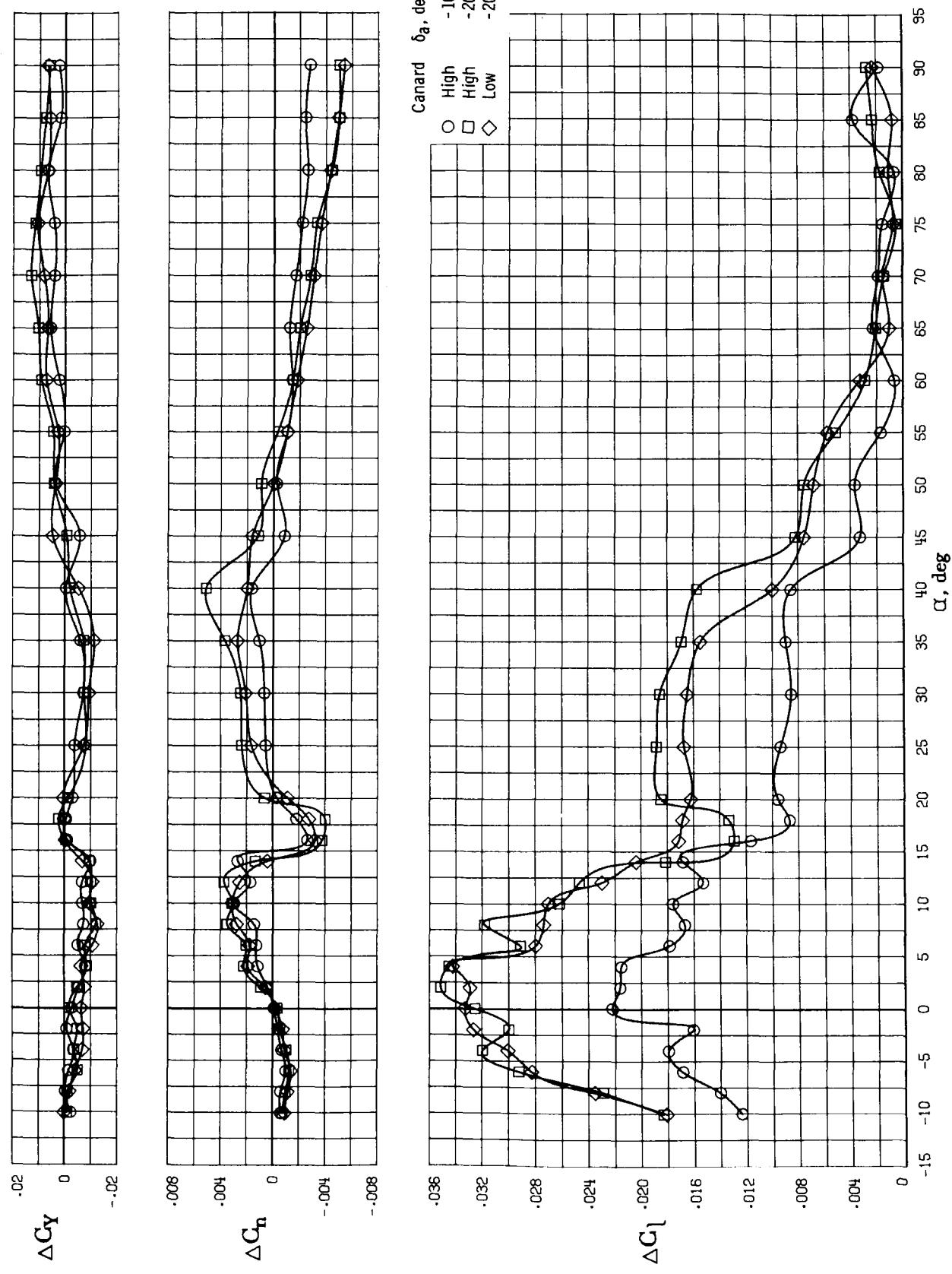
Figure 25. Aileron effectiveness of basic configuration. $\delta_e = 0°$; $i_c = 0°$.

46
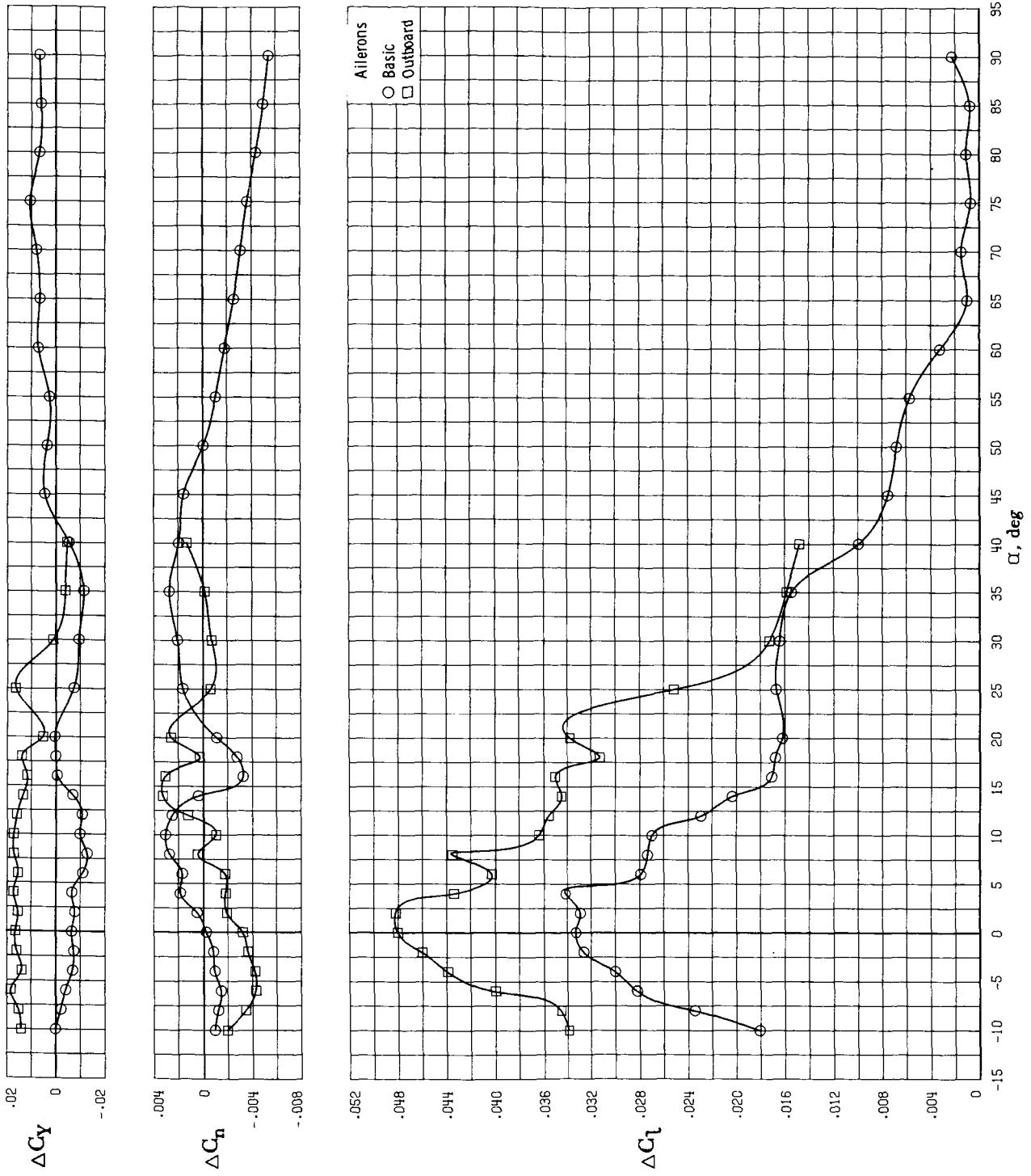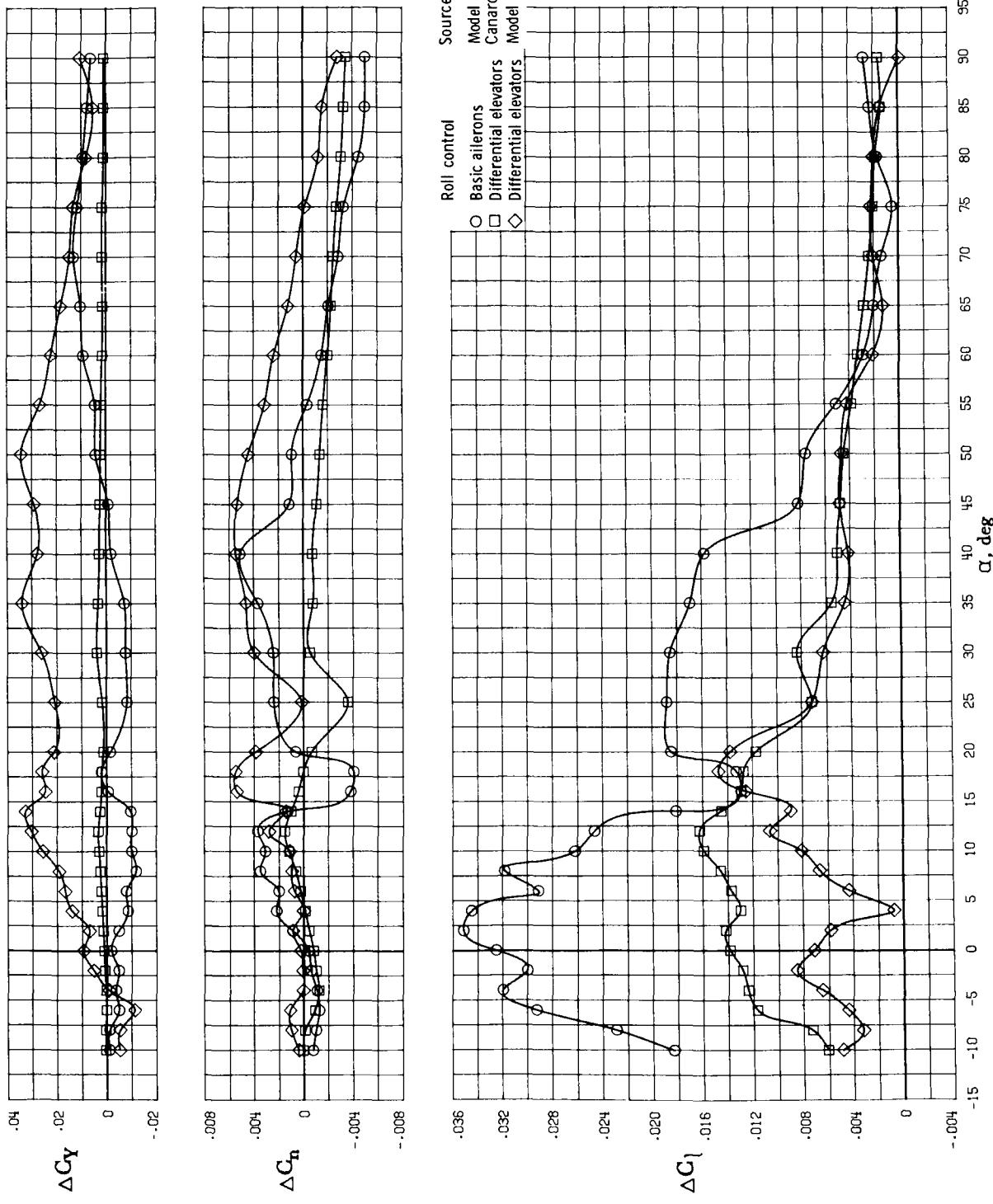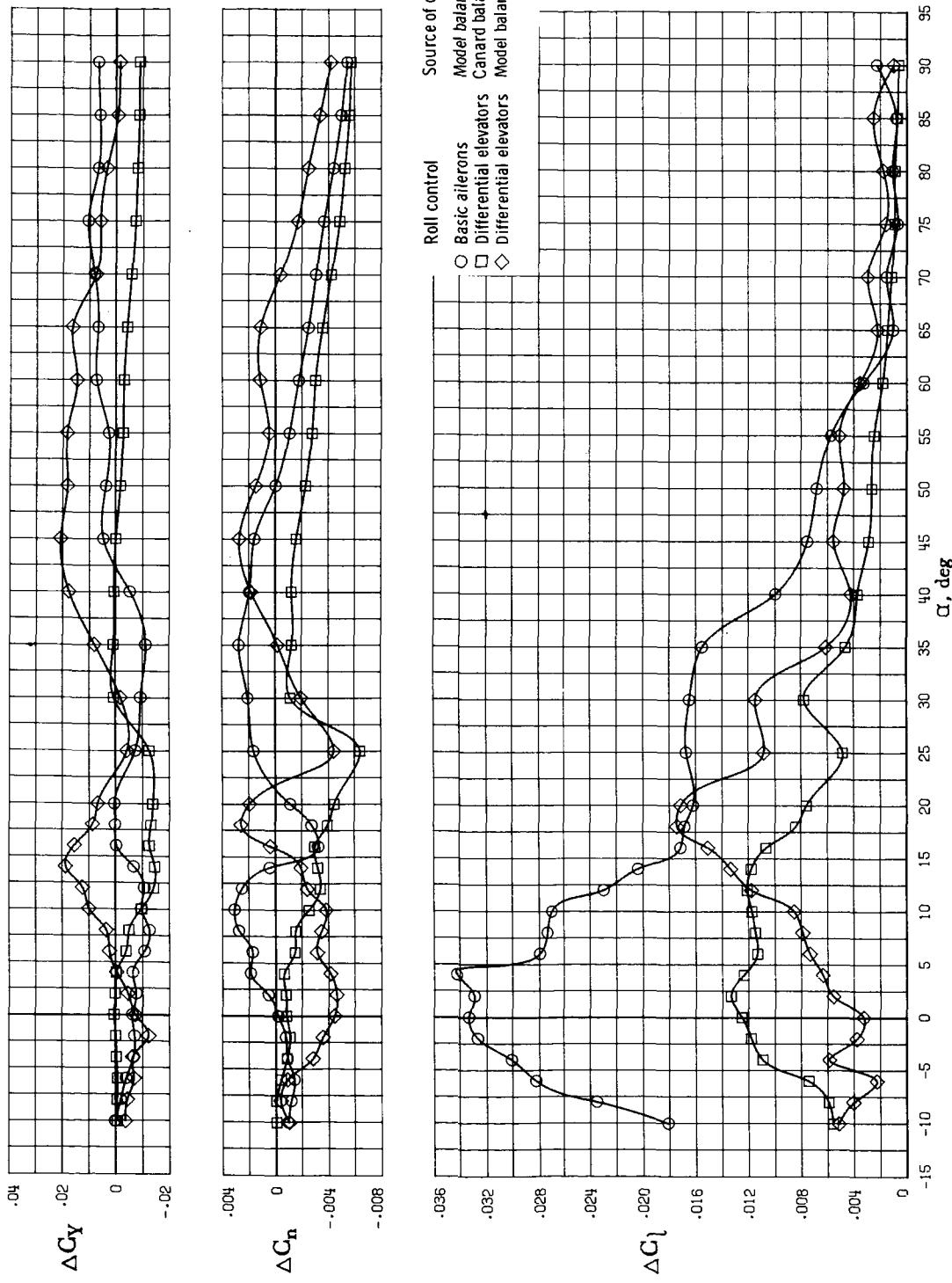
Figure 26. Comparison of effectiveness of outboard and basic aileron locations. $\delta_a = -20°$; low canard position; $\delta_e = 0°$; $i_c = 0°$.

Figure 27. Effectiveness of differential elevator deflection for roll control. $\delta_a = -20°$; $i_c = 0°$.

(a) High canard position.

48

(b) Low canard position.

Figure 27. Concluded.
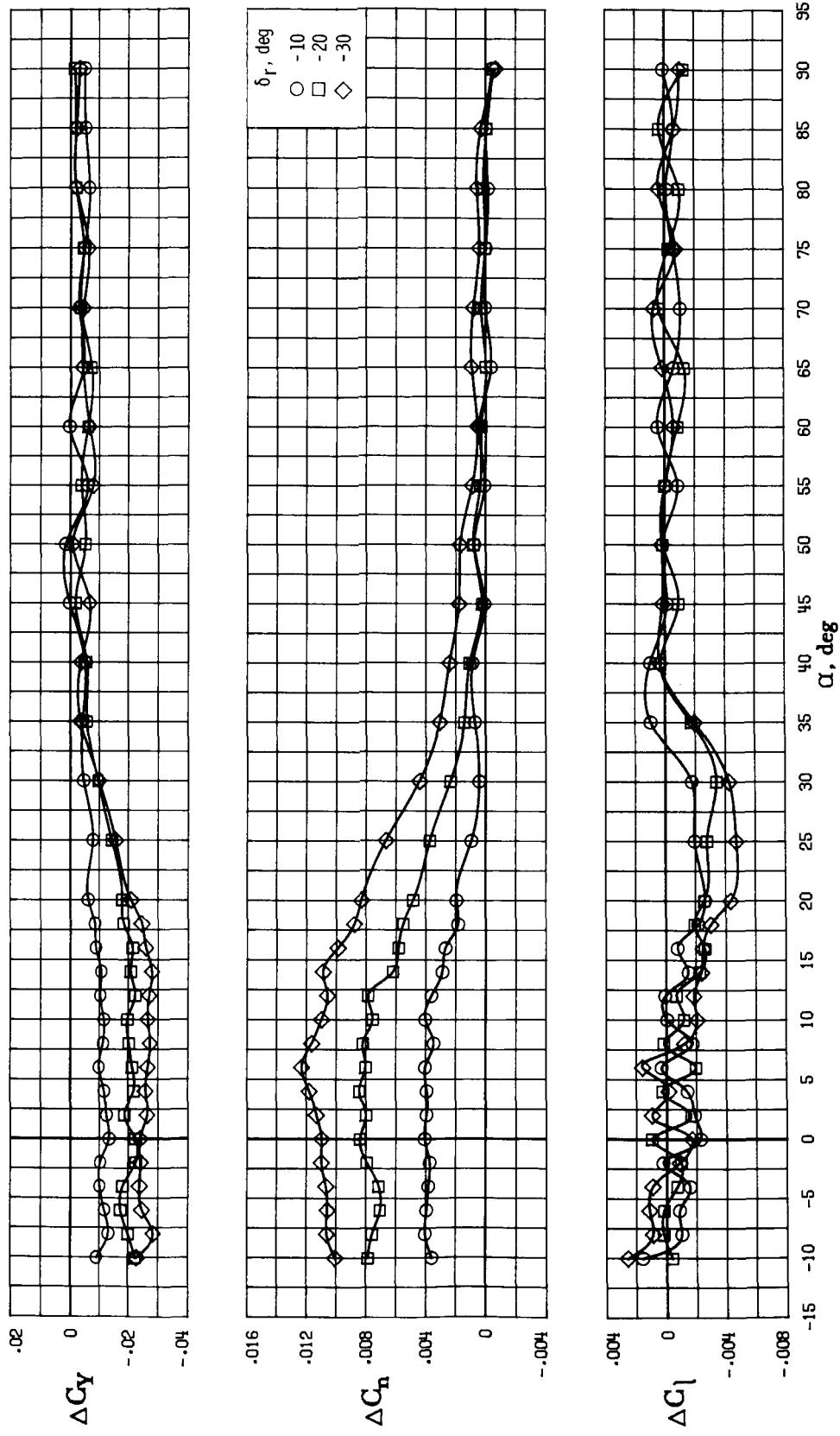
Figure 28. Rudder effectiveness of basic configuration. High canard position; $\delta_e = 0°$; $i_c = 0°$.
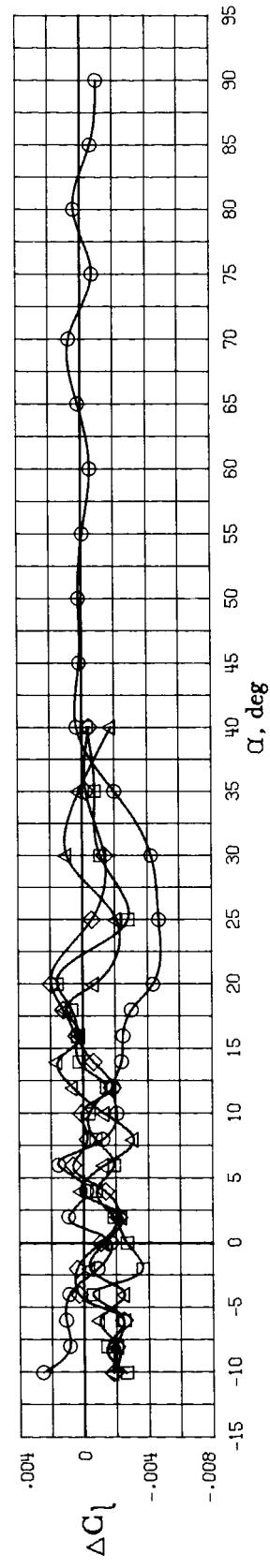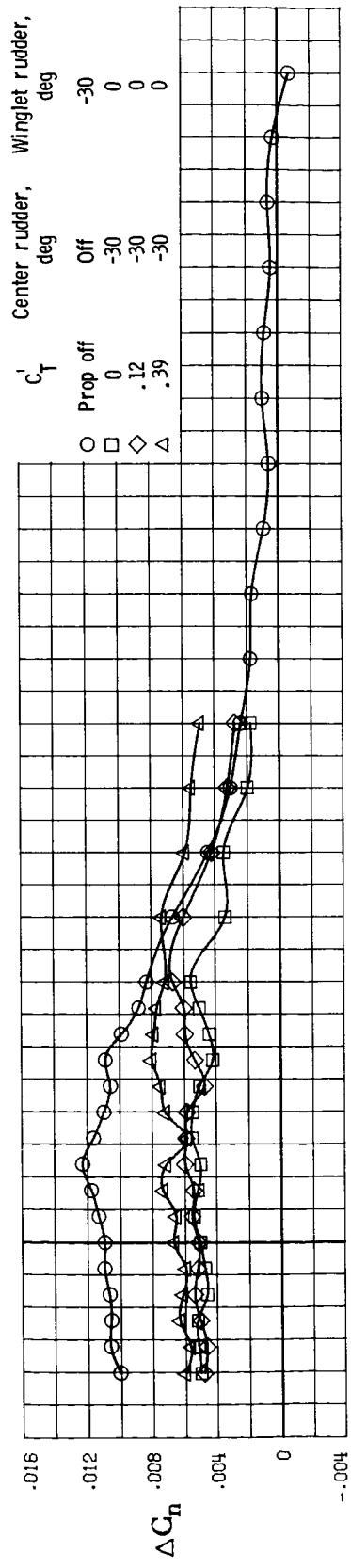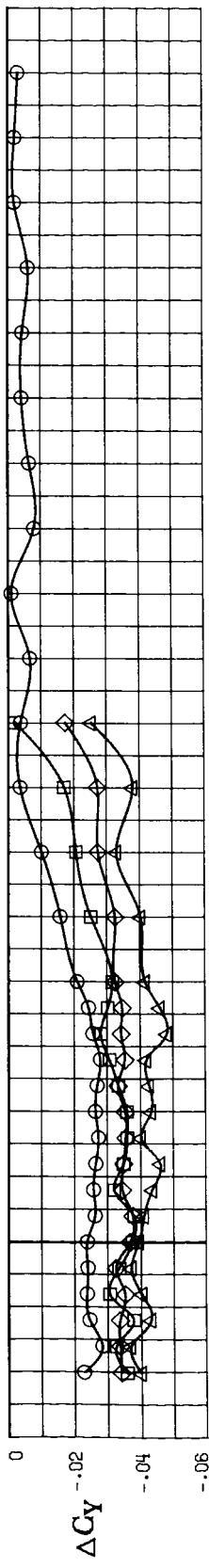
Figure 29. Comparison of effectiveness of added center rudder with basic rudder arrangement. Low canard; $\delta_e = 0^\circ$; $i_c = 0^\circ$.
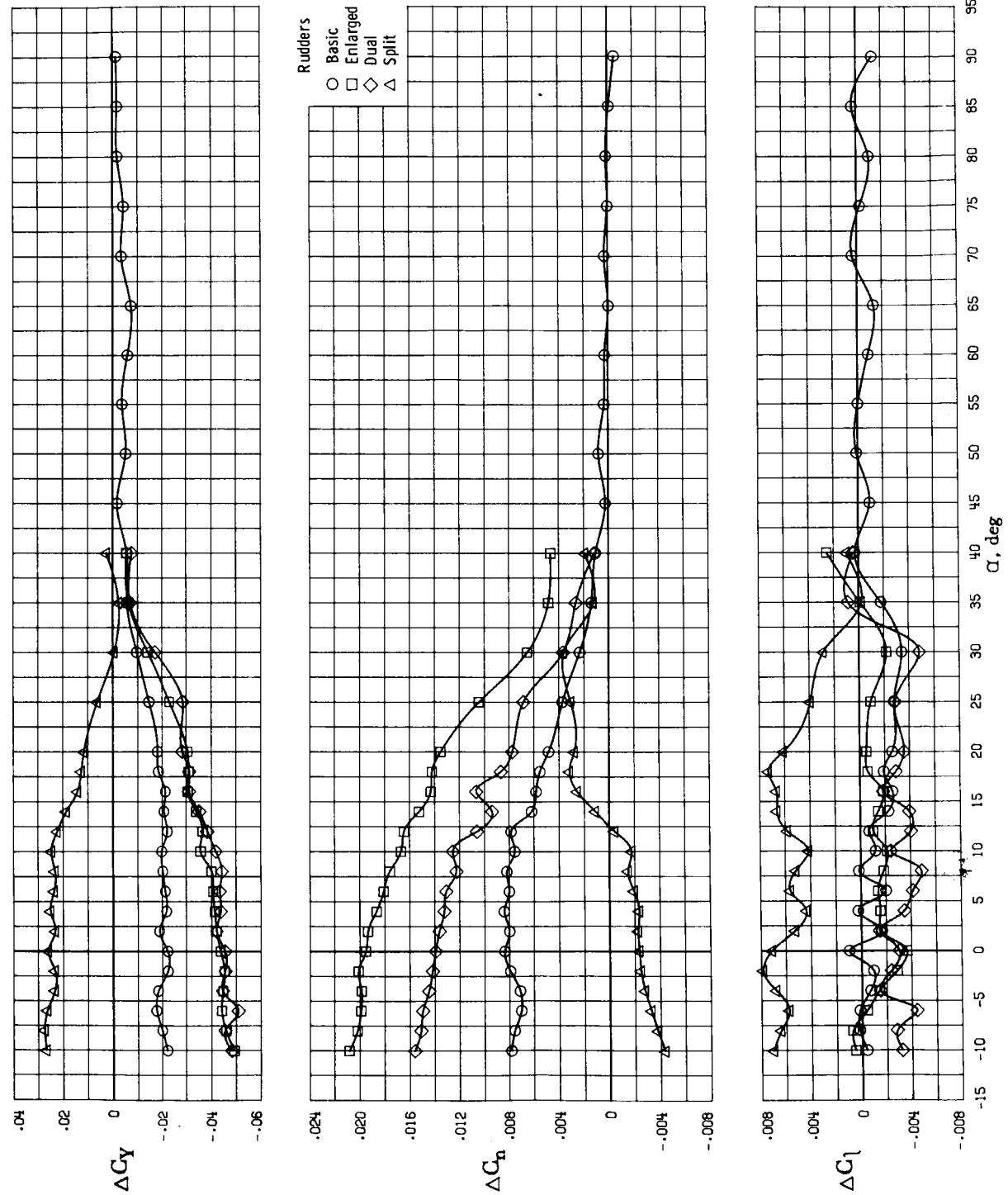
Figure 30. Comparison of effectiveness of modified winglet rudders with basic rudder arrangement. $\delta_r = -20°$; low canard; $\delta_e = 0°$; $i_c = 0°$.
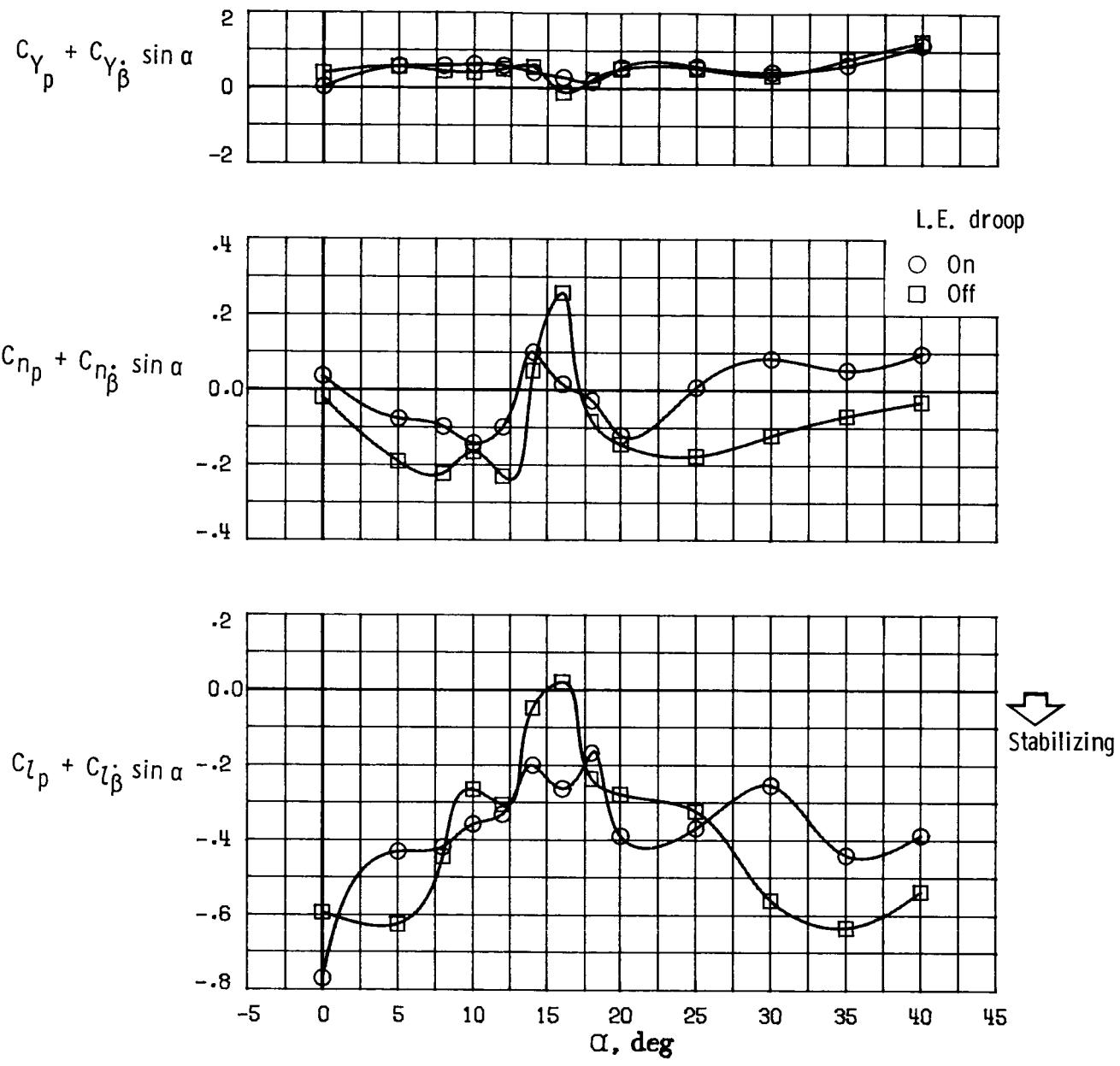
Figure 31. Effect of leading-edge droop on dynamic roll stability. High canard position; $\delta_e = 0°$; $i_c = 0°$.
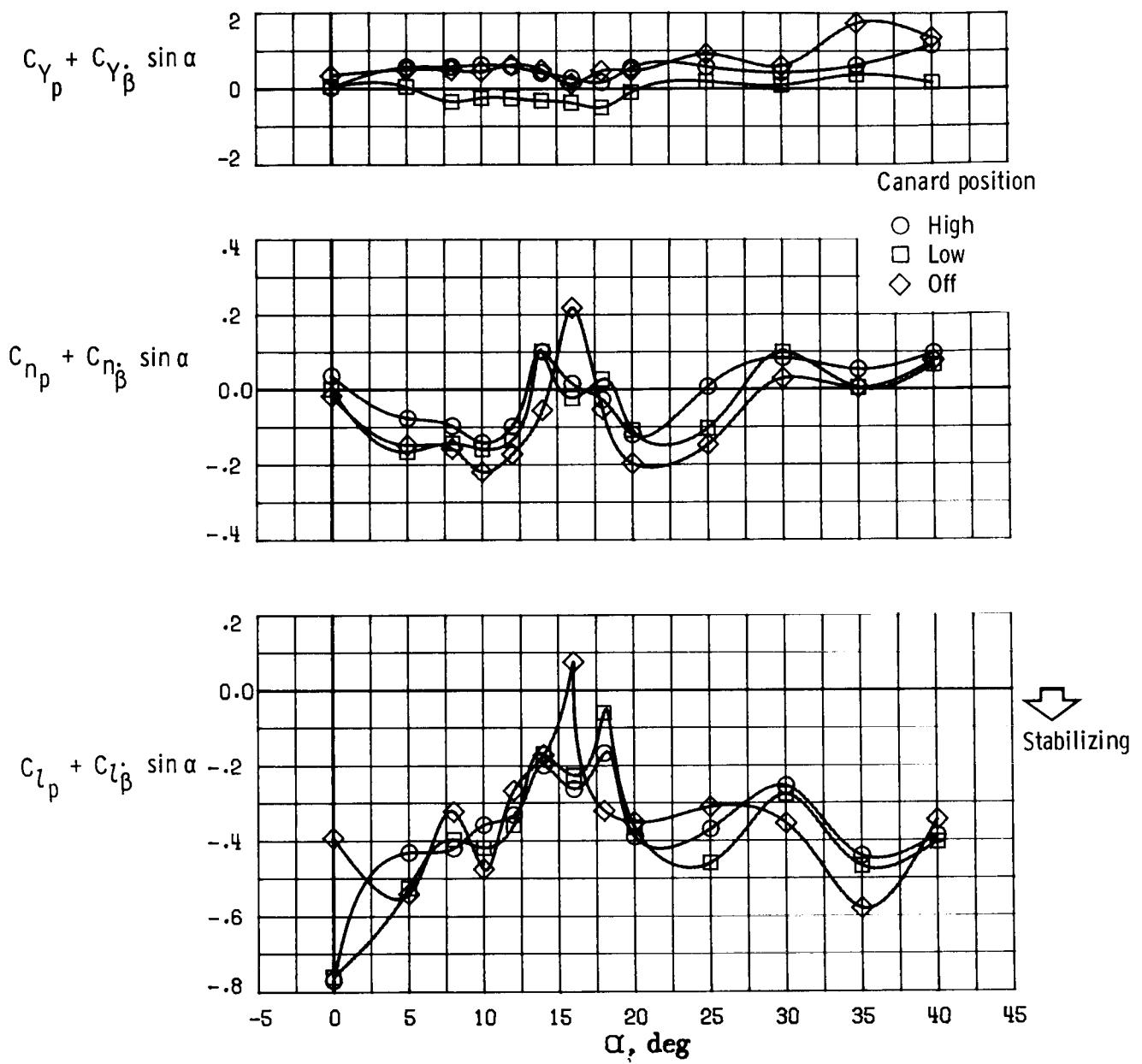
Figure 32. Effects of canard on damping in roll characteristics. Leading-edge droop on; $\delta_e = 0°$; $i_c = 0°$.
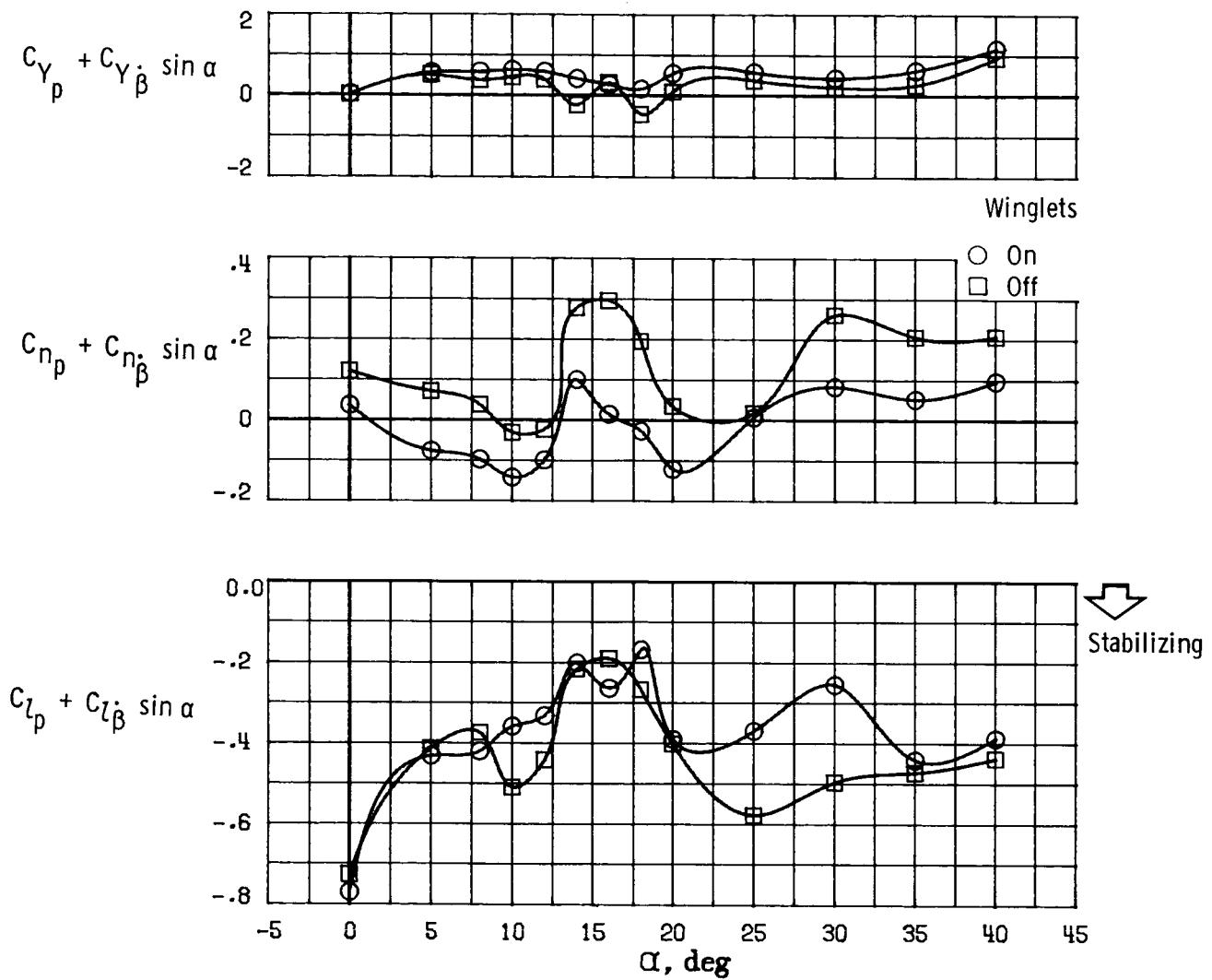
Figure 33. Effect of winglets on damping in roll characteristics. Leading-edge droop on; high canard position; $\delta_e = 0°$; $i_c = 0°$.
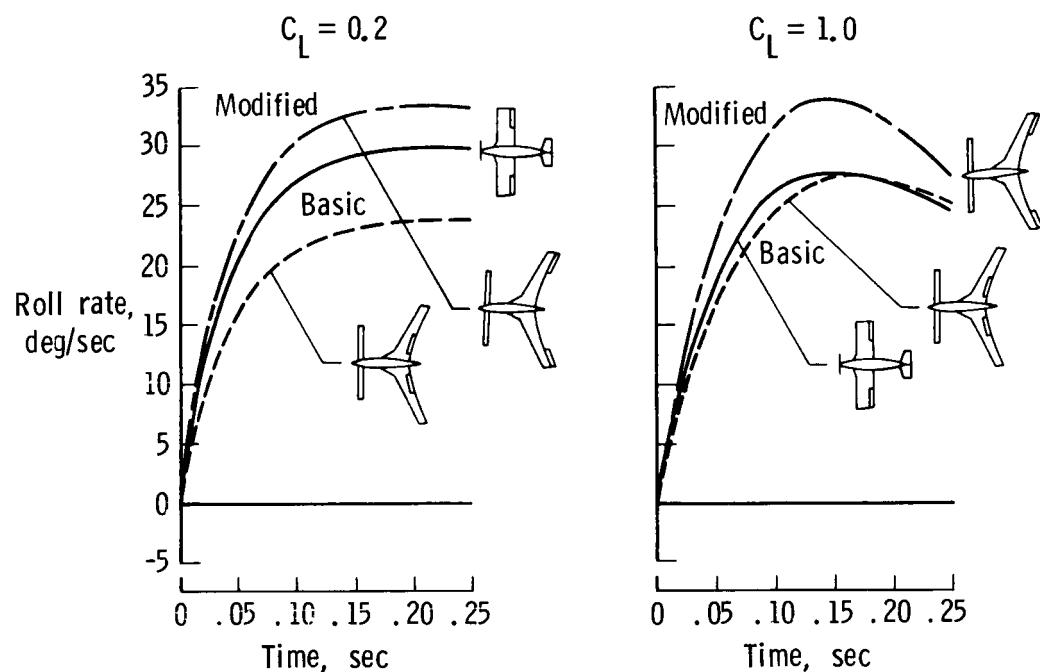
Figure 34. Comparison of calculated aileron response for conventional and canard designs.
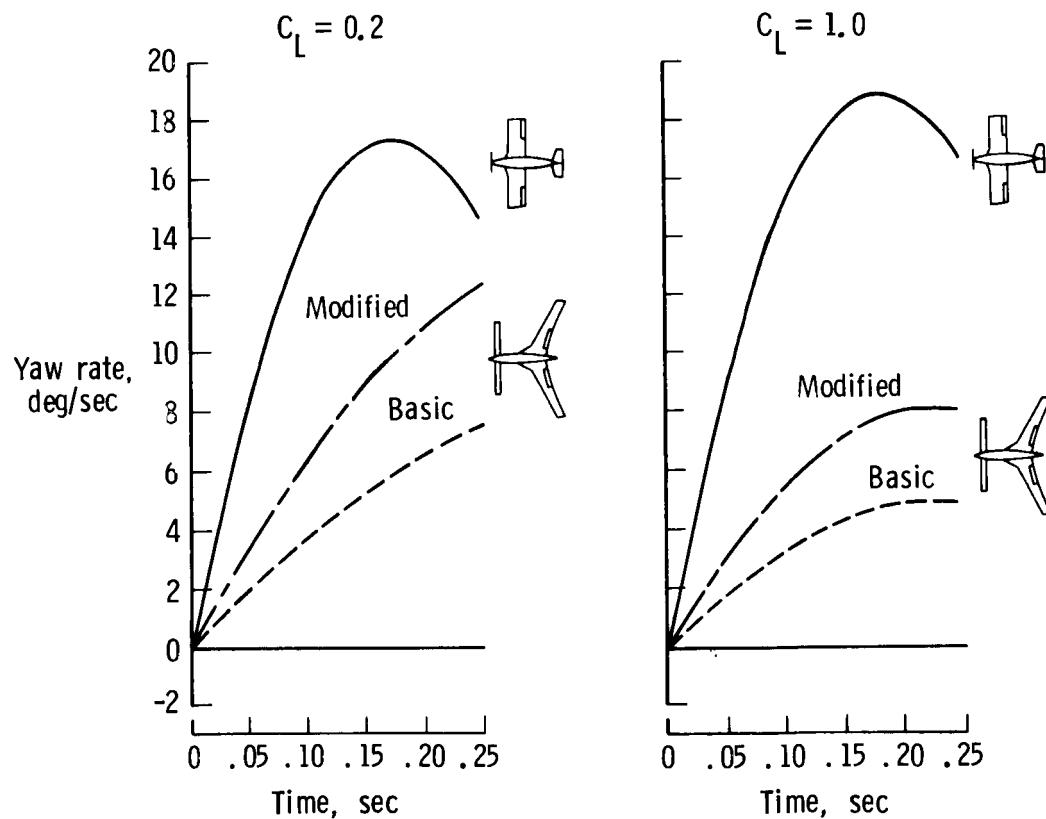
Figure 35 Comparison of calculated rudder response for conventional and canard designs.

Standard Bibliographic Page

1. Report No. NASA TP-2623	2. Government Accession No.	3. Recipient's Catalog No.	
4. Title and Subtitle Wind-Tunnel Investigation of the Flight Characteristics of a Canard General-Aviation Airplane Configuration		5. Report Date October 1986	
		6. Performing Organization Code 505-45-43-01	
7. Author(s) Dale R. Satran		8. Performing Organization Report No. L-15929	
9. Performing Organization Name and Address NASA Langley Research Center Hampton, VA 23665-5225		10. Work Unit No.	
		11. Contract or Grant No.	
12. Sponsoring Agency Name and Address National Aeronautics and Space Administration Washington, DC 20546-0001		13. Type of Report and Period Covered Technical Paper	
		14. Sponsoring Agency Code	
15. Supplementary Notes			

16. Abstract

A 0.36-scale model of a canard general-aviation airplane with a single pusher propeller and winglets was tested in the Langley 30- by 60-Foot Wind Tunnel to determine the static and dynamic stability and control and free-flight behavior of the configuration. Model variables made testing of the model possible with the canard in high and low positions, with increased winglet area, with outboard wing leading-edge droop, with fuselage-mounted vertical fin and rudder, with enlarged rudders, with dual deflecting rudders, and with ailerons mounted closer to the wing tips. The basic model exhibited generally good longitudinal and lateral stability and control characteristics. The removal of an outboard leading-edge droop degraded roll damping and produced lightly damped roll (wing rock) oscillations. In general, the model exhibited very stable dihedral effect but weak directional stability. Rudder and aileron control power were sufficiently adequate for control of most flight conditions, but appeared to be relatively weak for maneuvering compared with those of more conventionally configured models.

17. Key Words (Suggested by Authors(s)) Canard General aviation Stall/spin Stability and control Wing leading-edge modifications	18. Distribution Statement Unclassified—Unlimited Subject Category 02

19. Security Classif.(of this report) Unclassified	20. Security Classif.(of this page) Unclassified	21. No. of Pages 57	22. Price A04